

COMENIUS UNIVERSITY IN BRATISLAVA  
FACULTY OF MATHEMATICS, PHYSICS AND  
INFORMATICS



Using Graph Theory to Investigate  
Compensatory Mechanisms of the Ageing  
Brain

Diploma thesis

2025

Alena Usatova, BSc

COMENIUS UNIVERSITY IN BRATISLAVA  
FACULTY OF MATHEMATICS, PHYSICS AND  
INFORMATICS



# Using Graph Theory to Investigate Compensatory Mechanisms of the Ageing Brain

Diploma thesis

Study program:	Cognitive Science
Field of study:	Computer Science
Department:	Department of Applied Informatics
Supervisor:	Prof. RNDr. Ľubica Beňušková, PhD

Bratislava 2025

Alena Usatova



## THESIS ASSIGNMENT

**Name and Surname:** Alena Usatova  
**Study programme:** Cognitive Science (Single degree study, master II. deg., full time form)  
**Field of Study:** Computer Science  
**Type of Thesis:** Diploma Thesis  
**Language of Thesis:** English  
**Secondary language:** Slovak

**Title:** Using Graph Theory to Investigate Compensatory Mechanisms of the Aging Brain

**Annotation:** Analysis of the brain functional connectivity involves defining and quantifying functional links between predefined parts of the brain. Graph theoretical analysis of such functional networks derived from the fMRI data has proven to be instrumental in deepening our understanding of the brain activity.

**Aim:** Address three main questions: (1) Do older adults exhibit increased functional connectivity in the specific brain regions as a compensatory mechanism compared to younger adults? (2) Which brain regions show changes in the grey matter volume related to aging? (3) Is there any correlation between the graph theory metrics of functional connectivity and cognitive test scores in older adults?

**Literature:** Babayan, A., Erbey, M., Kumral, D. et al. (2019) A mind-brain-body dataset of MRI, EEG, cognition, emotion, and peripheral physiology in young and old adults. *Scientific Data* 6, DOI: 10.1038/sdata.2018.308  
Behfar, Q., Kambiz Behfar S., von Reutern, B. et al. (2020) Graph theory analysis reveals resting-state compensatory mechanisms in healthy aging and prodromal Alzheimer's disease. *Front. Aging Neurosci.* 12. DOI: 10.3389/fnagi.2020.576627  
McCarthy, P., Beňušková, L., Franz, E.A. (2014) The age-related posterior-anterior shift as revealed by voxelwise analysis of functional brain networks. *Front. Aging Neurosci.* DOI: 10.3389/fnagi.2014.00301

**Supervisor:** prof. RNDr. Ľubica Beňušková, PhD.  
**Department:** FMFI.KAI - Department of Applied Informatics  
**Head of department:** doc. RNDr. Tatiana Jajcayová, PhD.

**Assigned:** 15.05.2024

**Approved:** 15.06.2024

prof. Ing. Igor Farkaš, Dr.  
Guarantor of Study Programme

.....  
Student

.....  
Supervisor



### ZADANIE ZÁVEREČNEJ PRÁCE

**Meno a priezvisko študenta:** Alena Usatova  
**Študijný program:** kognitívna veda (Jednoodborové štúdium, magisterský II. st., denná forma)  
**Študijný odbor:** informatika  
**Typ záverečnej práce:** diplomová  
**Jazyk záverečnej práce:** anglický  
**Sekundárny jazyk:** slovenský

**Názov:** Using Graph Theory to Investigate Compensatory Mechanisms of the Aging Brain  
*Skúmanie kompenzačných mechanizmov starnúceho mozgu pomocou teórie grafov*

**Anotácia:** Analýza funkčnej konektivity mozgu zahŕňa definovanie a kvantifikovanie funkčných spojení medzi preddefinovanými časťami mozgu. Ukázalo sa, že analýza takýchto funkčných sietí odvodených z fMRI dát pomocou teórie grafov je neoceniteľná v prehľbovaní nášho porozumenia činnosti mozgu.

**Cieľ:** Preskúmajte tieto tri hlavné otázky: (1) Vykazujú starší dospelí zvýšenú funkčnú konektivitu v špecifických mozgových oblastiach ako kompenzačný mechanizmus v porovnaní s mladšími dospelými? (2) Ktoré mozgové oblasti vykazujú zmeny v objeme sivej hmoty v súvislosti so starnutím? (3) Existuje nejaká korelácia medzi grafovými mierami funkčnej konektivity a skóre kognitívnych testov u starších dospelých?

**Literatúra:** Babayan, A., Erbey, M., Kumral, D. et al. (2019) A mind-brain-body dataset of MRI, EEG, cognition, emotion, and peripheral physiology in young and old adults. *Scientific Data* 6, DOI: 10.1038/sdata.2018.308  
Behfar, Q., Kambiz Behfar S., von Reutern, B. et al. (2020) Graph theory analysis reveals resting-state compensatory mechanisms in healthy aging and prodromal Alzheimer's disease. *Front. Aging Neurosci.* 12. DOI: 10.3389/fnagi.2020.576627  
McCarthy, P., Beňušková, L., Franz, E.A. (2014) The age-related posterior-anterior shift as revealed by voxelwise analysis of functional brain networks. *Front. Aging Neurosci.* DOI: 10.3389/fnagi.2014.00301

**Vedúci:** prof. RNDr. Ľubica Beňušková, PhD.  
**Katedra:** FMFI.KAI – Katedra aplikovanej informatiky  
**Vedúci katedry:** doc. RNDr. Tatiana Jajcayová, PhD.

**Dátum zadania:** 15.05.2024

**Dátum schválenia:** 15.06.2024

prof. Ing. Igor Farkaš, Dr.  
garant študijného programu

.....  
študent

.....  
vedúci práce

## **Declaration**

I hereby declare that I elaborated this diploma thesis independently using cited literature

Bratislava, 2025

.....

## **Acknowledgements**

I would like to express my sincere gratitude to my supervisor, Prof. RNDr. Lúbia Beňušková, PhD, for her wise advice, support, guidance, and for giving me the freedom to choose the topic and methods of this thesis. I am also deeply grateful to my family and friends for their encouragement and for believing in me when I did not believe in myself. Finally, I would also like to thank all the faculty members at the Master's Programme in Cognitive Science at Comenius University for the knowledge they shared, the support they provided and for maintaining a community that inspires learning and exploration.

## **Abstract**

This study investigated whether increased functional connectivity in specific brain regions in older adults serves as a compensatory mechanism. Drawing on cognitive ageing theories, which state that compensatory activity helps maintain performance despite age-related decline, we tested three criteria for compensation: (1) whether regions with increased functional connectivity are involved in cognitive functions, (2) whether these regions show grey matter loss, and (3) whether functional connectivity correlates with cognitive performance.

The study included three age groups: Group 1 (N = 79; 25 females, 54 males; aged 20–25 years), Group 2 (N = 75; 20 females, 55 males; aged 25–40 years, median age group 25–30), and Group 3 (N = 73; 37 females, 36 males; aged 55–80 years, median age group 65–70).

Resting-state fMRI data from three age groups were analysed using graph-theoretical metrics, focusing on the degree centrality (DC). Structural MRI data were used to assess grey matter volume, and the results in the cognitive tests were correlated with changes in DC. Older adults showed increased degree centrality in the frontal and parietal regions, which are associated with attention, memory, and reasoning. However, these regions did not exhibit grey matter reduction or significant correlations with cognitive performance.

Thus, although age-related changes in brain structure and functional network topology were evident, the results did not meet the criteria for compensatory mechanisms. This differs from findings from clinical populations in previous studies, suggesting that compensation may be more pronounced in the presence of pathology.

## Abstrakt

Táto štúdia skúmala, či zvýšená funkčná konektivita v špecifických oblastiach mozgu starších dospelých slúži ako kompenzačný mechanizmus. Vychádzajúc z teórií kognitívneho starnutia, ktoré uvádzajú, že kompenzačná aktivita pomáha udržať výkon napriek vekovo podmienenému poklesu, testovali sme tri kritériá kompenzácie: (1) či oblasti so zvýšenou funkčnou konektivitou sú zapojené do kognitívnych funkcií, (2) či tieto oblasti vykazujú stratu šedej hmoty a (3) či funkčná konektivita koreluje s kognitívnym výkonom.

Štúdia zahŕňala tri vekové skupiny: Skupina 1 (N = 79; 25 žien, 54 mužov; vek 20–25 rokov), Skupina 2 (N = 75; 20 žien, 55 mužov; vek 25–40 rokov, medián vekovej skupiny 25–30) a Skupina 3 (N = 73; 37 žien, 36 mužov; vek 55–80 rokov, medián vekovej skupiny 65–70).

Dáta z resting-state fMRI zo všetkých troch vekových skupín boli analyzované pomocou grafoteoretických metrik, so zameraním na stupňovú centrálnosť (degree centrality, DC). Štrukturálne MRI dáta slúžili na hodnotenie objemu šedej hmoty a výsledky kognitívnych testov boli korelované so zmenami DC. Starší dospelí vykázali zvýšenú stupňovú centrálnosť v čelových a parietálnych oblastiach, ktoré sú spojené s pozornosťou, pamäťou a uvažovaním. Avšak tieto oblasti nevykazovali zníženie šedej hmoty ani významné korelácie s kognitívnym výkonom.

Napriek tomu, že boli zrejme vekovo podmienené zmeny v štruktúre mozgu a topológii funkčných sietí, výsledky nespĺňali kritériá kompenzačných mechanizmov. Toto sa líši od zistení v klinických populáciách v predchádzajúcich štúdiách, čo naznačuje, že kompenzácia môže byť výraznejšia v prítomnosti patológie.

# Contents

<b>1</b>	<b>INTRODUCTION .....</b>	<b>13</b>
1.1	AGEING .....	13
1.1.1	<i>Searching for a Definition .....</i>	<i>13</i>
1.1.2	<i>Functional Connectivity Patterns in the Ageing Brain .....</i>	<i>15</i>
1.1.3	<i>Theories of Cognitive Ageing .....</i>	<i>16</i>
1.2	OVERVIEW OF FUNCTIONAL AND STRUCTURAL NETWORK ANALYSES AND GRAPH THEORY IN NEUROSCIENCE.....	18
1.2.1	<i>Brain Connectivity.....</i>	<i>18</i>
1.2.2	<i>Graph Theory.....</i>	<i>21</i>
1.3	THE AIM OF THE RESEARCH, RESEARCH QUESTIONS, AND HYPOTHESIS .....	23
<b>2</b>	<b>METHODS.....</b>	<b>25</b>
2.1	PARTICIPANTS .....	25
2.2	MRI ACQUISITION AND PREPROCESSING .....	26
2.3	GRAPH THEORY ANALYSIS .....	29
2.4	GREY MATTER VOLUME ANALYSIS .....	31
2.5	COGNITIVE PERFORMANCE CORRELATION .....	32
<b>3</b>	<b>RESULTS .....</b>	<b>34</b>
3.1	ROIS WITH A SIGNIFICANT INCREASE IN DC BETWEEN GROUPS.....	34
3.2	ROI MORPHOMETRIC ANALYSIS OF THE GREY MATTER .....	36
3.3	CORRELATION ANALYSIS BETWEEN ROIS WITH INCREASED DC AND COGNITIVE TESTS .....	38
3.4	GLOBAL EFFICIENCY, LOCAL EFFICIENCY, CLUSTERING COEFFICIENT, CHARACTERISTIC PATH LENGTH, AND DECREASED DEGREE CENTRALITY .....	39
<b>4</b>	<b>DISCUSSION .....</b>	<b>45</b>
4.1	INTERPRETATION OF KEY FINDINGS.....	45
4.2	LIMITATIONS .....	50
4.3	FUTURE WORK.....	51
4.4	INTERDISCIPLINARITY .....	52
<b>5</b>	<b>CONCLUSION.....</b>	<b>53</b>
<b>6</b>	<b>BIBLIOGRAPHY .....</b>	<b>55</b>
<b>APPENDIX A</b>	<b>BRAINNETOME ATLAS SUBREGIONS TABLE .....</b>	<b>62</b>
<b>APPENDIX B</b>	<b>REGIONS OF INTEREST WITH A SIGNIFICANT DIFFERENCE IN DEGREE CENTRALITY BETWEEN OLDER ADULTS AND YOUNGER ADULTS .....</b>	<b>68</b>
<b>APPENDIX C</b>	<b>REGIONS OF INTEREST WITH A SIGNIFICANT DIFFERENCE IN DEGREE CENTRALITY BETWEEN OLDER ADULTS AND EARLY MIDDLE-AGED ADULTS .....</b>	<b>70</b>

APPENDIX D	REGIONS OF INTEREST WITH A SIGNIFICANT DIFFERENCE IN GLOBAL EFFICIENCY BETWEEN OLDER ADULTS AND YOUNGER ADULTS .....	72
APPENDIX E	REGIONS OF INTEREST WITH A SIGNIFICANT DIFFERENCE IN GLOBAL EFFICIENCY BETWEEN OLDER ADULTS AND EARLY MIDDLE-AGED ADULTS.....	74
APPENDIX F	REGIONS OF INTEREST WITH A SIGNIFICANT DIFFERENCE IN LOCAL EFFICIENCY BETWEEN OLDER ADULTS AND YOUNGER ADULTS .....	76
APPENDIX G	REGIONS OF INTEREST WITH A SIGNIFICANT DIFFERENCE IN LOCAL EFFICIENCY BETWEEN OLDER ADULTS AND EARLY MIDDLE-AGED ADULTS.....	77
APPENDIX H	REGIONS OF INTEREST WITH A SIGNIFICANT DIFFERENCE IN CLUSTERING COEFFICIENT BETWEEN OLDER ADULTS AND YOUNGER ADULTS .....	78
APPENDIX I	REGIONS OF INTEREST WITH A SIGNIFICANT DIFFERENCE IN CLUSTERING COEFFICIENT BETWEEN OLDER ADULTS AND EARLY MIDDLE-AGED ADULTS.....	79
APPENDIX J	REGIONS OF INTEREST WITH A SIGNIFICANT DIFFERENCE IN AVERAGE PATH DISTANCE BETWEEN OLDER ADULTS AND YOUNGER ADULTS .....	80
APPENDIX K	REGIONS OF INTEREST WITH A SIGNIFICANT DIFFERENCE IN AVERAGE PATH DISTANCE BETWEEN OLDER ADULTS AND EARLY MIDDLE-AGED ADULTS .....	82

# List of Figures

<b>FIGURE 1.1.</b> MRI IMAGES OF A 58-YEAR-OLD FEMALE PATIENT WITH A HIGH-GRADE GLIAL TUMOUR AND GLIOMATOSIS CEREBRI.....	19
<b>FIGURE 1.2.</b> (A) WORKFLOW OF VOXEL-BASED MORPHOMETRY (VBM) ANALYSIS. (B) DATA FLOW IN FUNCTIONAL CONNECTIVITY ANALYSIS. ....	20
<b>FIGURE 1.3.</b> ILLUSTRATION OF KEY NETWORK CENTRALITY MEASURES.....	22
<b>FIGURE 2.1.</b> NUMBER OF MALE AND FEMALE PARTICIPANTS IN EACH AGE GROUP. ....	26
<b>FIGURE 2.2.</b> COMPARISON OF POWER SPECTRAL DENSITY (PSD) ACROSS DIFFERENT PREPROCESSING APPROACHES.....	28
<b>FIGURE 2.3.</b> AVERAGE GLOBAL COST EFFICIENCY (GCE) PLOTTED AGAINST NETWORK COST (COST) ACROSS ALL SUBJECTS. ....	30
<b>FIGURE 3.1.</b> GROUP DIFFERENCES IN THE DEGREE CENTRALITY (DC) VISUALISED ON THE 3D BRAIN MODELS USING THE CONN TOOLBOX. ....	35
<b>FIGURE 3.2.</b> GREY MATTER VOLUME DIFFERENCES IN SELECTED ROIS BASED ON THE BRAINNETOME ATLAS.....	37
<b>FIGURE 3.3.</b> GREY MATTER (GM) VOLUME AS A FUNCTION OF TOTAL INTRACRANIAL VOLUME (TIV) ACROSS AGE GROUPS..	38
<b>FIGURE 3.4.</b> CORRELATION BETWEEN DEGREE CENTRALITY IN THE RIGHT PARAHIPPOCAMPAL GYRUS (BN_ATLAS_246.CLUSTER110) AND VERBAL FLUENCY IN OLDER ADULTS (GROUP 3).....	39
<b>FIGURE 3.5.</b> GROUP DIFFERENCES IN THE GLOBAL EFFICIENCY (GE) VISUALISED ON 3D BRAIN MODELS USING THE CONN TOOLBOX. ....	40
<b>FIGURE 3.6.</b> GROUP DIFFERENCES IN THE LE VISUALISED ON THE 3D BRAIN MODELS USING THE CONN TOOLBOX. ....	42
<b>FIGURE 3.7.</b> GROUP DIFFERENCES IN CC VISUALISED ON 3D BRAIN MODELS USING THE CONN TOOLBOX. ....	43
<b>FIGURE 3.8.</b> GROUP DIFFERENCES IN THE CHARACTERISTIC PATH LENGTH (PL) VISUALISED ON 3D BRAIN MODELS USING THE CONN TOOLBOX. ....	44

## List of abbreviations

aMTG – anterolateral middle temporal gyrus  
ATN – anterior thalamic nuclei  
BF – basal forebrain  
CC – clustering coefficient  
DC – degree centrality  
DMN – default mode network  
DTI – Diffusion Tensor Imaging  
FC – functional connectivity  
FPN – frontoparietal network  
fMRI – functional magnetic resonance imaging  
GE – global efficiency  
GLM – general linear models  
HAROLD – hemispheric asymmetry reduction in older age  
ICA – independent component analysis  
IFG – regions of the inferior frontal gyrus  
MD – mediodorsal thalamic nuclei  
M – modularity  
mPFC – medial prefrontal cortex  
MRI – Magnetic Resonance Imaging  
PASA – posterior-anterior shift in ageing  
PCC – posterior cingulate cortex  
PFC – prefrontal cortex  
PL – average path distance  
ROI – regions of interest  
rs-fMRI – resting-state functional magnetic resonance imaging  
SC – structural connectivity  
sMRI – structural magnetic resonance imaging  
SMA – supplementary motor area  
SN – salience network  
vmPFC – the ventromedial prefrontal cortex  
VBM – voxel-based morphometry

# 1 Introduction

## 1.1 Ageing

The World Health Organisation (WHO) reports on the steady growth of the older population, which predicts that 1 in 6 people in the world will be over 60 years old by 2030, and the size of this group will increase from 1 billion to 1.4 billion. The number of people aged 80 and above is set to triple by 2050, reaching 426 million (WHO, 2022). As can be seen, the world will confront the challenge when countries experience an additional burden on their economies, healthcare systems, as well as social sectors.

Older people themselves will go through significant changes that might impact their quality of life and overall satisfaction. Advancing through age can be characterised by physical alterations such as joint stiffness and decrease in flexibility, loss of muscle mass and strength, slower metabolism, the development of chronic diseases, and other factors. Cognitive functions are also subject to deterioration. However, it is common to classify them into crystallised and fluid abilities, as they exhibit opposite progression throughout the lifespan. Crystallised abilities refer to acquired knowledge and skills that are accumulated over their lifetime. Conversely, fluid abilities do not depend on prior knowledge and experience, focusing instead on solving novel reasoning problems. Studies indicate that while crystallised abilities tend to increase until around the age of 60, plateauing until 80, fluid abilities show a declining trajectory starting from early adulthood and continuing throughout life (Murman, 2015). Maintaining cognitive and physical strength is crucial for preserving the independence of the ageing population. Therefore, significant measures must be implemented to overcome these challenges, particularly those that are directed at supporting individuals and improving their physical and mental well-being.

### 1.1.1 Searching for a Definition

Ageing is studied from various perspectives by different scientific domains, such as gerontology, evolutionary biology, genetics, epidemiology, demographics, neuroscience, and others. As a result, there are many definitions of ageing. Thus, demography focuses on analysing records at regular intervals of the number of deceased individuals and their age, until the entire cohort passes away. It allows for the analysis of survival and mortality patterns (Bronikowski, 2010). Although this idea is often linked to a person's chronological age in society, it is not directly correlated with it, as the notion of a "typical" older person does not accurately reflect the diversity of ageing experiences. Evolutionary biology defines ageing as a

multifaceted feature that stems from evolutionary biology adaptation, including various factors rather than being a singular physiological process (Rose *et al.*, 2012). Although physiology is not the only aspect, it constitutes a pivotal part of the definition. Twelve key age-related physiological traits have been outlined in mammals: genomic instability, telomere attrition, epigenetic alterations, loss of proteostasis, disabled macroautophagy, deregulated nutrient-sensing, mitochondrial dysfunction, cellular senescence, stem cell exhaustion, altered intercellular communication, chronic inflammation, and dysbiosis (López-Otín *et al.*, 2023). As these changes occur at the molecular and cellular levels of an organism, the brain is likewise susceptible to them.

One of the possible definitions of brain ageing in neuroscience describes it as a complex network of processes, characterised by multifaceted mechanisms that include both localised changes and factors from a broader systematic context (Gaspar-Silva, Trigo and Magalhaes, 2023). The authors highlight in their review the same cellular mechanisms as those that were proposed by López-Otín *et al.* (2023), within the broader context encompassing the processes of the entire organism. However, even with a rapidly growing body of research, it is still not clear whether these factors are causes or effects of ageing. The fact that different tissues are susceptible to alterations related to age with different rates suggests an interconnection between the central nervous system and the periphery (Gaspar-Silva, Trigo and Magalhaes, 2023). Thus, the complexity of the aspects contributing to the understanding of brain ageing continues to grow. The authors highlight that decreased myelination of axon fibres that project to distant regions of the brain might affect communication between them and deteriorate the overall network communication. The integrity of neuronal, axonal, glial, and neurotransmitting functioning is crucial for the maintenance of network operation and cognition.

With the development of neuroimaging techniques, such as functional magnetic resonance imaging (fMRI) and diffusion tensor imaging (DTI), a broad scope of research has emerged to explore functional connectivity (FC) and structural connectivity (SC) within the brain. This approach conceptualises the brain as interconnected patterns of neural activations organised in networks. These patterns can be analysed at micro-, meso-, and macroscale levels. It is worth noticing that connectivity relies on the structure, but SC is neither a sufficient nor a complete constraint (Friston, 2011). The molecular and cellular changes might affect both age-related deterioration of grey matter and white matter (Giorgio *et al.*, 2010), resulting in structural modifications, and functional alterations in various brain regions. Therefore, studies examining variations in functional connections across the lifespan are considered to be beneficial in interpreting age-related brain reorganisations.

### 1.1.2 Functional Connectivity Patterns in the Ageing Brain

Over the recent few decades, research on the ageing brain and FC has gained widespread recognition. Data have been obtained from cross-sectional and longitudinal studies, as well as task-based and resting-state designs. For instance, the results from the population-based Rotterdam Study (Zonneveld *et al.*, 2019) involving 2878 healthy individuals aged between 50 and 95 years demonstrated a significant decline in within-network connectivity associated with older age in the anterior default mode network (DMN), ventral attention network, and sensorimotor network. Conversely, an increase in FC was observed in the visual network. Furthermore, between-network connectivity showed patterns of both increased and decreased (anti-) correlations. A longitudinal study in a group of healthy 16 ageing individuals (mean age =  $74.38 \pm 4.52$ ) over 4 years reported a decline in FC within the frontoparietal network (FPN), and the salience network (SN), while no change in the DMN (Oschmann and Gawryluk, 2020). Meanwhile, another longitudinal investigation analysed 34 cognitively normal subjects (mean age =  $78.27 \pm 3.14$ ) over 4 years and demonstrated a reduction in FC in the DMN, and the dorsal attention network (DAN), and an increase in the left insular and left supplementary motor area (SMA) (Li *et al.*, 2020). Varangis Burns, Habeck and Stern (2020) examined the effects of ageing on FC in 11 tasks reflecting 4 cognitive domains (vocabulary, processing speed, fluid reasoning, and episodic memory). They found that task choice can significantly influence the results of FC analysis. The decline in within-network connectivity correlates with age, although the cognitive task can alter the presence and magnitude of the effects. It also revealed a decrease in between-network FC with age. The variations in the investigation outcomes can be attributed to the methodological approaches employed. For example, the choice of the region-based versus whole-brain connectivity analysis or the selection of the parcellation technique will significantly affect the results.

Overall, the substantial scope of evidence from rs-fMRI research implies the modifications in the whole-brain connectivity patterns as well as within some large-scale networks (Sala-Llonch, Bartrés-Faz and Junqué, 2015). In this review, the authors highlighted the overall reduction of FC in older adults compared to young ones, emphasising the difference in the trajectory of the changes in tasks and at rest. In a systematic review by Deery *et al.* (2023) on resting-state functional networks, findings revealed a decline in within-network and increased between-network FC associated with age. Moreover, older adults demonstrated diminished segregation and modularity of the brain regions, as well as decreased hub function and lateralisation, alongside a shift from posterior to anterior brain activity. These results align with prevailing theories of cognitive ageing. Although the main hypotheses were formulated to

explain changes in task performance, they are also applicable to the resting-state patterns of alteration.

### 1.1.3 Theories of Cognitive Ageing

It may be reasonable to highlight two main hypotheses of cognitive ageing, as they serve as the basis for other frameworks designed to illustrate conceptual models of brain ageing. Firstly, *the dedifferentiation framework*, proposed in the first half of the twentieth century, suggests that cognitive abilities differentiate in early adolescence, maintain through adulthood, and dedifferentiate in late life (Hülür *et al.*, 2015). When applied from a network perspective, brain regions demonstrate more diffused, less selective, and specific interactions. It may indicate the ability of structurally distinct components of the network system to comparably contribute to a particular outcome, offering functional flexibility (Deery *et al.*, 2023). Secondly, *the compensatory hypothesis* assumes that older subjects recruit higher levels of functional activation to maintain comparable performance under increasing task demands, which may serve as a compensational mechanism for age-related alterations (Reuter-Lorenz and Cappell, 2008). The prefrontal regions usually display the highest overactivation in seniors.

Indeed, two pivotal phenomena of age effects on the brain known as HAROLD and PASA might be noticeable manifestations of dedifferentiation and compensation. The hemispheric asymmetry reduction in older age (HAROLD) describes a tendency of reduction in lateralisation of the brain activity during task performance in the PFC in older individuals (Cabeza, 2002). The posterior-anterior shift in ageing (PASA) represents an age-related decrease of the activity in the occipitotemporal regions of the brain. At the same time, there is a corresponding increase in the frontal areas.

Drawing upon the hypotheses described above, *the scaffolding theory of ageing and cognition (STAC)* views ageing as a negative interplay of such indices as functional deterioration and neural challenges. External factors that can have both positive and negative effects on the brain function and structure, combined with a beneficial process called compensatory scaffolding. The deterioration related to the atrophy of GM and WM, depletion of dopamine, and maladaptive brain activity is counteracted by the activation of additional neural pathways, which provide extra computational support (Reuter-Lorenz and Park, 2014). The model was revised based on the evidence from multiple studies by adding a variable called the life course of ageing that allows the experience, education, genetics, and environment to directly influence brain function and structure as well as the compensatory scaffolding.

Another framework that took into account the discrepancy between age-related changes and pathology was proposed by Stern (2012). *The Cognitive reserve (CR)* concept suggests that

the application of pre-existing cognitive strategies in the brain will aid in confronting pathological states occurring with age or disease even when the brain reserve is constant. Therefore, individuals with a higher cognitive reserve are expected to experience fewer adverse effects of damage, which was supported by extensive epidemiological and later neuroimaging studies. Subjects with higher levels of education, occupational attainment, and engagement in diverse leisure activities are associated with longer-maintained cognitive performance in later life.

*The theory of coordination dynamics* proposed by Tognoli and Kelso (2014) describes the dynamics of cognitive, behavioural, and social functions as real-time coordination supported by metastability. Metastable dynamics is a key mechanism that enables the coexistence of the tendency of brain regions to maintain a balance between segregating their specialised functions and simultaneously integrating multiple functions (Deery *et al.*, 2023).

Taken together, despite the differences in applied analytical approaches and multidirectional patterns of brain network activation, general patterns associated with age can be distinguished. There is a significant deterioration in different cognitive domains related to older age, such as executive functions, memory, and processing speed. Structural and functional modifications are present in the ageing brain. Although the underlying mechanisms are still not fully understood, the empirical evidence for the changes in grey and white matter integrity, amyloid deposits, vascular disease, and dopamine depletion implies the alteration in the brain structure that, in turn, can be a contributing but not sufficient factor for alterations in brain functioning. The findings from fMRI studies reveal an overall decrease in within-network FC and enhanced between-network connectivity patterns. The functional network organisation displays a major shift in activation from posterior to anterior areas, overactivation in some regions, as well as lateralisation in the hemispheres which might serve as compensatory mechanisms of the ageing brain. These changes may exhibit linear and positive (U-shaped) and negative quadratic trajectories in FC across the lifespan depending on the inter- or intra-connections among the networks. The inflexion points are usually observed in about the fourth or fifth decades of life. Starting from early adulthood, when networks display more segregated and functionally localised region activation, they transition to more interconnected network interactions. One of the most extensively reported networks associated with the ageing brain is the DMN, which appears to be one of the most compromised networks with age. FC between the DMN areas decreases with the progression of age, although the correlation with other networks grows stronger.

## 1.2 Overview of Functional and Structural Network Analyses and Graph Theory in Neuroscience

### 1.2.1 Brain Connectivity

The human brain is comprised of almost one hundred billion interconnected neurons along with glial cells, which makes it one of the most complex systems. This creates an exceptionally challenging endeavour to understand the mechanisms underlying cognitive and behavioural functions. Therefore, it is reasonable to conceptualise the organisation of the brain as a network-based architecture. The units may represent individual or ensembles of neurons exhibiting various interconnected patterns. However, it is important to distinguish between different types of these links.

*Structural connectivity* (SC) represents physical connections between brain regions via white matter tracts. *Functional connectivity* (FC) is the *coordinated information exchange of spatially separated brain regions* in order to allow integrative and higher-order functions. *Functional connectivity* is defined as the temporal dependency of neuronal activation patterns of anatomically separated *brain regions*. *Effective connectivity*, in turn, aims to establish causal interactions between units by measuring the directional influence of one neural population on another (Erol and Hunyadi, 2022). Each approach reveals different properties of connections between neural populations, which makes it beneficial to consider a combination of various analytical techniques to analyse such multifactorial processes as ageing.

#### 1.2.1.1 Structural Connectivity

The common technique for quantitatively measuring SC is diffusion-weighted MRI (DWI), which uses strong diffusion-sensitising magnetic gradients as part of the pulse sequence to analyse water diffusion of WM (see **Figure 1.1**, reproduced from Figure 5 in Karaarslan and Arslan, 2008). Various magnetic field gradients are applied to measure how water molecules move. If water diffuses freely in the medium between two gradient pulses, the phase shift occurs, and the net magnetisation changes, leading to dephasing and a reduction in net magnetisation, which results in a signal loss in the direction of the gradient. To acquire more detailed information from DWI, the Diffusion Tensor Imaging (DTI) model is used. It provides information about the magnitude and directionality of water molecule movement. The key indices that are extracted from a tensor include Mean Diffusivity (MD), Fractional Anisotropy (FA), Axial Diffusivity (AD), and Radial Diffusivity (RD) (Jones, 2010).

Research on changes in SC across the lifespan revealed that FA, which indicates the preferable directionality of diffusion, decreases with age. Meanwhile, MD, a measure of overall

diffusion strength, and RD, a myelin integrity marker, increase with age (Westlye *et al.*, 2010). On the other hand, there is a strong concern about interpreting the results of these metrics as reliable indicators of SC. Several factors can modulate the direction of diffusion anisotropy: the axon diameter distribution, the axon density, and, specifically, how axons are spatially related to each other within one voxel. If axons are oriented in multiple directions within a single voxel, it will lead to a reduced FA index, although it may reflect a fibre complexity rather than a reduction in structural connectivity (Jones, 2010).

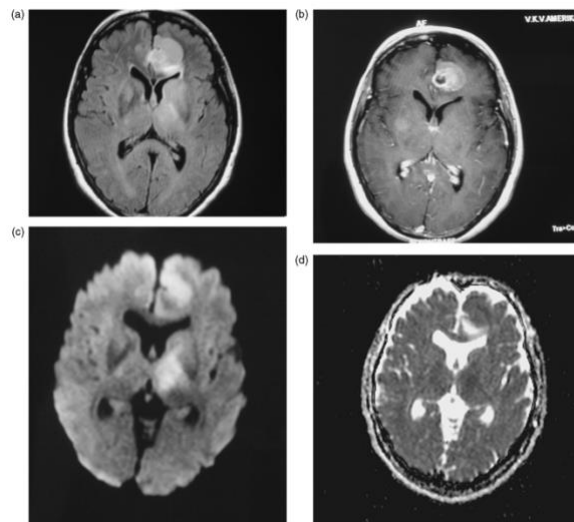


**Figure 1.1.** MRI images of a 58-year-old female patient with a high-grade glial tumour and gliomatosis cerebri. (a) FLAIR sequence shows tumoral infiltration in the left cingulate gyrus and bilateral basal ganglia; (b) Post-contrast T1-weighted image reveals enhancement in the same regions; (c) Diffusion-weighted image (DWI) shows high signal intensity; (d) Apparent diffusion coefficient (ADC) map indicates increased diffusivity (reproduced from Karaarslan and Arslan (2008), Figure 5)

Another common technique for analysing structural imaging is voxel-based morphometry (VBM), which measures the variation in GM (as shown in **Figure 1.2 A**, reproduced from Figure 1 in Kurth, Luders and Gaser, 2015). It enables a voxel-wise comparison of the volume of GM between two groups of subjects. Its advantage is that it thoroughly evaluates the anatomical differences across the entire brain without being limited to a specific structure. It represents a statistical comparison of segmented GM volumes (Ashburner and Friston, 2000). In the study comparing older adults (N = 14, mean age = 71) to a middle-aged group (N = 16, mean age = 41), the results revealed a reduction of GM volume in the frontal, temporal, parietal and occipital regions (areas associated with executive functions and language) along with decreased performance in the related cognitive test (Ramanoël *et al.*, 2018).

#### 1.2.1.2 *Functional Connectivity*

It is common to classify methods into model-based and model-free approaches. In model-based connectivity, one or more regions of interest (ROI) are selected to identify a link between these

regions and the rest of the network. The connections are established based on the predefined parameters such as the number of regions, statistical thresholds, and the assumption of a linear relationship in FC. Connectivity matrices can be built using the cross-correlation approach, which is typically applied without considering phase shifts between signals due to its high computational cost (as illustrated in **Figure 1.2 B**, reproduced from Figure 3 in Milano, Guzzi and Cannataro, 2019). However, these methods may show high correlations driven by physiological artefacts, such as breathing and cardiac rhythms. The coherence approach is developed to mitigate this issue. Statistical parametric mapping uses General Linear Models (GLM) to identify regional brain activation patterns and Gaussian random field theory to account for multiple comparisons. It was originally used for task-based fMRI, but it was also adopted for rs-fMRI. Model-free analysis does not require any prior knowledge of specific regions and can be useful for identifying non-linear relationships (Farahani, Karwowski and Lighthall, 2019). It is carried out using either decomposition techniques, such as principal component analysis and independent component analysis (ICA), or clustering methods, such as hierarchical clustering, fuzzy c-means, and mutual information (Kucikova *et al.*, 2023).

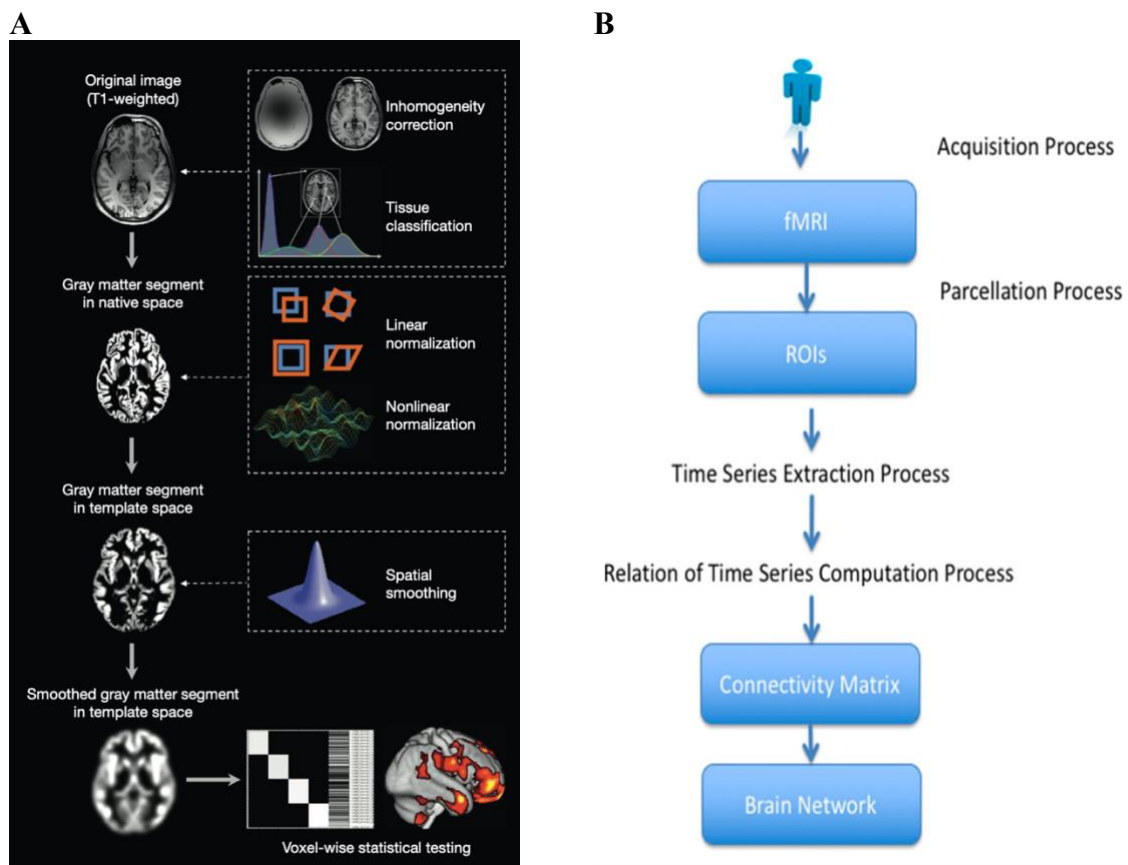


**Figure 1.2.** (A) *Workflow of voxel-based morphometry (VBM) analysis.* High-resolution T1-weighted images are bias-corrected, segmented into tissue types, and grey matter maps are normalised to a standard template. After smoothing, statistical tests are applied voxel-wise to identify significant effects (reproduced from Kurth, Luders and Gaser (2015), Figure 1). (B) *Data flow in functional connectivity analysis.* fMRI data are first parcellated into brain regions, from which time series are extracted. Functional connections (edges) are then computed between region pairs to construct a connectivity matrix (reproduced from Milano, Guzzi and Cannataro (2019), Figure 3).

## 1.2.2 Graph Theory

Graph theory is extensively applied across numerous disciplines, including physics, biology, chemistry, social sciences, and more. It is no surprise that network science has been embraced by neuroscience, as it offers tools for topological description, quantitative analysis, and understanding the complexity of network organisations.

The implementation of this method is based on the idea that the brain can be modelled by the graph of interconnected nodes. Depending on the purposes of the analysis, nodes can represent an individual neuron, a group of neurons, or a brain region. They can be defined on functional or structural data parcellation, or derived using data-driven methods, such as boundary detection and clustering patterns of connectivity. Edges in the graph correspond to the connections between these nodes. They can have binary or weighted values, where binary values indicate the presence or absence of a connection, and weighted values assign the strength to the connection. They can also be directed or undirected, providing a directional relationship between the nodes (Sporns, 2018). A correlation matrix is generated after applying one of the connectivity methods and determining the threshold. This allows the application of various graph metrics to analyse the network's topology.

According to Rubinov and Sporns (2010), most measures can be classified as global and local. Those which describe individual elements of the network are considered to exhibit local properties, and the distribution of elements reveals network-level characteristics. Global measures can provide insights into how the network is organised, including functional segregation and integration of information flow. Segregation determines how strongly the elements are grouped into distinct clusters. Functional segregation reflects specialised neural processing, while structural segregation shows the possibility of functional segregation. The basic measures that quantify it are the *clustering coefficient (CC)* and *modularity (M)*. CC shows the proportion of nodes' neighbours that are also connected (as seen in **Figure 1.3**, reproduced from Figure 3 in Tanglay *et al.*, 2023). M assesses the strength of community structure, measuring how well the network is divided into modules with dense intra-group and sparse inter-group connections.

Integration shows how effectively the network facilitates global information flow. *Path length (PL)* measures the average distance between nodes. In SC, it can identify the network's potential for functional integration between regions. However, in FC, it does not directly quantify the information flow and must be interpreted with caution. The metric of functional integration is the *characteristic path length*, indicating the average shortest path length. *Global efficiency (GE)* is its inverse index, which characterises how efficiently the network facilitates information exchange.

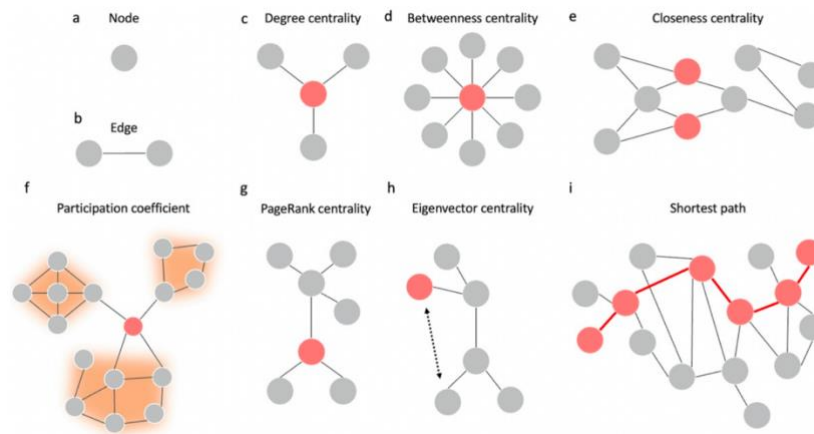


**Figure 1.3.** Illustration of key network centrality measures. Brain nodes (a) are connected by structural or functional edges (b). Examples include degree (c), betweenness (d), closeness (e), participation coefficient (f), PageRank (g), and eigenvector centrality (h), each highlighting different aspects of a node's importance. Path length (i) reflects network efficiency (reproduced from Tanglay et al. (2023), Figure 3).

Small-worldness (SM) is another well-known characteristic that describes the balance between segregation and integration. The topology of such a network can demonstrate high clustering among neighbours and short average path lengths. Yet, this single statistic should not be used in isolation to measure segregation and integration, as functional networks exhibit higher segregation but lower integration in comparison to anatomical networks.

Measures of centrality evaluate the importance of nodes in the network. Nodes with high degree are considered as hubs. The *degree* indicates how many connections a node has, while other various metrics, such as the *within-modular degree z-score*, *participation coefficient*, *closeness centrality*, and *betweenness centrality*, describe other aspects of node importance. However, they can have different interpretations, regarding functional and structural networks. Since FC reveals statistical dependencies among regions rather than direct anatomical connections, path-based measures may not always reflect the node's structural significance as a facilitator of information flow, as functional connections can be independent of physical pathways.

*The assortativity coefficient* is a graph metric that quantifies the tendency of nodes to connect to other nodes with similar degree. The positive correlation indicates that the network has resilient interconnected high-degree hubs. The negative correlation shows the widely distributed and vulnerable hubs.

It is important to mention that network architecture depends on the network's basic elements, such as the number of nodes, edges, and degree distributions. To obtain meaningful statistics, the networks should be compared to a null-hypothesis network, a baseline with the same network elements (e.g., degree distributions) but random connections, (Rubinov and Sporns, 2010).

Farahani, Karwowski and Lighthall (2019) in the systematic review, note that some studies have shown that age-related changes in brain networks, which are associated with the alterations in highly connected hub areas of the DMN, attentional, sensorimotor, and visual networks in rs-fMRI. Local efficiency and the rich club coefficient increased until adulthood but declined with ageing, while global efficiency remained unchanged. The inverse trajectory of long and short connections suggests continuous network reorganisation over time. Modularity presents inconsistent results, with some studies reporting minimal change and others indicating a linear decrease. An intriguing finding was that intra-modular communication increased during a semantic decision-making task, while inter-modular communication was more pronounced at rest, a pattern also observed in the language network. Moreover, the nodal degree of the DMN correlated with cognitive performance when comparing a resting state with an attentional task.

### 1.3 The aim of the research, research questions, and hypothesis

The brain is not an invariant system; rather, its fundamental nature is to be highly adaptive and responsive to changes in the environment and the body's internal state. However, how these alterations occur throughout the lifespan remains unclear. According to the prevailing view, the decline in cognitive abilities is inversely related to age. At the same time, some evidence indicates that the trajectory of these relations can depict negative quadratic patterns, with peak performance occurring in the fourth decade. Meanwhile, these processes do not occur in all regions simultaneously. On the contrary, activity decreases in some regions while others exhibit increases (see Section 1.1.2). In the compensatory hypothesis, these mechanisms are thought to compensate for the age-related changes in structural connectivity. Regions demonstrate less selective interactions within networks and increased integration between them (see Section 1.1.3).

Although the model of compensation has been widely utilised in the literature, it remains poorly defined, as its definition depends on the level of analysis to which it is applied. Behfar *et al.*, (2020) proposed four criteria to indicate compensatory mechanisms in the resting-state studies. First, the functional connectivity of the region must increase significantly. Second, this brain region must simultaneously exhibit a decline in neural integrity. Third, this region must be associated with cognitive functions. Fourth, to distinguish compensatory activation from random or maladaptive activation, the increase in functional connectivity must be positively correlated with cognitive performance. Research indicated a compensatory effect in participants with mild cognitive impairment but not in healthy senior controls. The lack of significant correlation between the degree centrality (DC) and cognitive test scores might reflect weaker

compensation in the ageing population, as the changes are not as profound as in the clinical population, or it might be a result of the limited size of this group.

This study aims to investigate age-related differences in network organisation and their compensatory effects on the network organisation by assessing differences in functional and structural connectivity patterns and their correlation with cognitive performance in older and younger adults. We are posing the following questions:

1. Do older adults exhibit increased functional connectivity in specific brain regions associated with cognitive functions as a compensatory mechanism compared to younger adults?
2. Do those brain regions demonstrate a reduction in GM volume in older adults?
3. Is there any correlation between the graph theory metrics of functional connectivity in those regions and cognitive test scores in older adults?

## 2 Methods

Our study uses the MPI-Leipzig Mind-Brain-Body (LEMON) publicly available dataset, which includes multimodal data from healthy participants across different ages (*MPI-Leipzig\_Mind-Brain-Body - OpenNeuro, 2017*). The data were acquired cross-sectionally for 227 volunteers in Leipzig, Germany, between 2013 and 2015 to study the mind-body-emotion interaction (Babayan *et al.*, 2019). The dataset provides a variety of neuroimaging data, psychological measures, demographic data, cognitive tests and physiological measures, but for the purpose of this research, only the Magnetic Resonance Imaging (MRI) data and cognitive tests were used. The LEMON data were collected consistently with the Declaration of Helsinki and with approval of the local ethical committee at the medical faculty of the University of Leipzig.

Data acquisition occurred over two rounds. On the first day, participants underwent structural and functional MRI scanning using a 3 Tesla Siemens Magnetom Verio scanner. Sequences included resting-state fMRI, quantitative T1-weighted MP2RAGE, T2-weighted, FLAIR, SWI/QSM, and DWI imaging. Cardiovascular parameters (heart rate, blood pressure, respiration) were continuously monitored during resting-state fMRI. Additional assessments included anthropometrics, blood sampling, and urine drug screening.

On the second assessment day, participants completed a resting-state EEG session and a battery of psychological assessments covering cognitive performance, emotional and personality traits, and psychiatric symptoms. Instruments included the Standardised Clinical Interview for DSM IV, Hamilton Depression Scale, Borderline Symptoms List, and various standardised questionnaires.

### 2.1 Participants

The full sample consisted of 227 participants divided into a younger group (N = 153, 45 females, 108 males, age range: 20 – 35 years, mean age = 25.1, SD = 3.1) and an older group (N = 74, 37 females, 37 males, age range: 59 – 77 years, mean age = 67.6, SD = 4.7), as can be seen in **Figure 2.1**. However, for the purposes of our study, we split the subjects into three age groups: Group 1 (N = 79, 25 females, 54 males, 20–25 years), Group 2 (N = 75, 20 females, 55 males, age range 25-40, median group is 25-30), and Group 3 (N = 73, 37 females, 36 males, age range 55-80 years, median group is 65-70 years). This grouping was chosen first of all to capture more subtle differences in the effect of ageing on the brain and second to maintain approximately the same number of participants in each group to preserve the statistical power.. The exact age of the subjects is not provided in the study; rather, they are grouped into age

ranges. Participants were recruited through public advertisements and university networks. The recruitment was conducted in two phases: a telephone pre-screening using a semi-structured interview and a subsequent on-site screening conducted by study physicians to ensure no exclusion criteria were met.

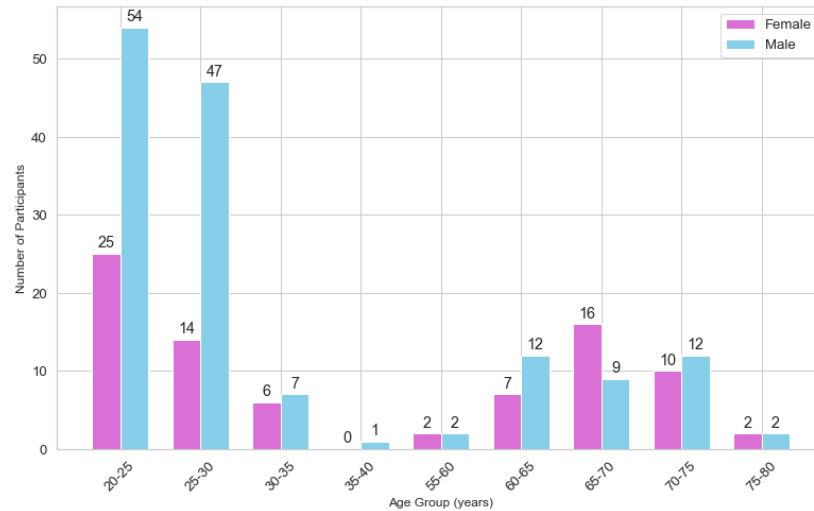


**Figure 2.1.** Number of male and female participants in each age group. Each bar represents the number of individuals in a specific age group, separated by gender: blue bars correspond to male participants and pink bars to female participants.

## 2.2 MRI Acquisition and Preprocessing

The MRI data were acquired using a 3 Tesla Siemens MAGNETOM Verio scanner (Siemens Healthcare GmbH, Erlangen, Germany) equipped with a 32-channel head coil. The scanning protocol remained stable throughout the data collection period, with no major maintenance or software updates affecting data consistency.

Functional images were acquired using a T2\*-weighted multiband echo planar imaging (EPI) BOLD sequence. Acquisition parameters were: TR = 1400 ms; total volumes = 657; total acquisition time = 15 minutes 30 seconds. Images were angulated  $-15^\circ$  from the AC-PC line to optimise coverage. During rs-fMRI, participants were instructed to remain awake, keep their eyes open, and fixate on a low-contrast cross. Although no physiological confirmation of wakefulness was collected, participants were asked to stay awake throughout the scan. To correct for geometric distortions, gradient echo field maps and two pairs of reversed phase-encoded spin echo images were acquired.

A Magnetisation-Prepared 2 Rapid Acquisition Gradient Echoes (MP2RAGE) sequence was acquired for high-resolution structural imaging (1 mm isotropic). These T1-weighted images, free from confounding influences such as proton density and T2\*, are optimal for morphometric analyses (e.g., cortical thickness, voxel-based morphometry). Acquisition time

for MP2RAGE was 8 minutes 22 seconds. Additionally, a standard T2-weighted volume (1 mm isotropic) was acquired in 4 minutes 43 seconds.

The preprocessing steps were implemented in the FMRIB Software Library (FSL; Smith *et al.*, 2004; Jenkinson *et al.*, 2012) and the CONN software (Nieto-Castanon, 2020; Nieto-Castanon and Whitfield-Gabrieli, 2022). Although the LEMON study provides for the analysis both the raw data and preprocessed data, we chose to work with the raw data and design a custom preprocessing pipeline according to the objectives of our research questions.

There is no golden standard preprocessing pipeline that could be adopted for rs-fMRI; the optimal approach, if such exists, depends on both the characteristics of the study population and the specific research objectives. Notably, the choice and the order of the preprocessing steps can significantly affect the outcomes of functional connectivity analysis and graph metrics (Aurich *et al.*, 2015). In our study, we compared participants from different age groups, including adults over 70 years old. Previous research has shown that older adults tend to exhibit head motion during scanning, which can lead to false correlations in functional connectivity metrics (Kato *et al.*, 2020). Such motion-related artefacts can be especially problematic for graph analysis, as they may change the structure of the network by artificially increasing the number of nodes and edges. Another topic of ongoing debate in the neuroimaging community is the use of global signal regression (GSR). GSR is used to reduce noise by removing signals that are shared across the whole brain. However, this step, by removing shared variance across the brain, moves the mean of the distribution towards zero, which can introduce negative correlations and alter true relationships between the regions (Saad *et al.*, 2012). Thus, GSR should be applied with caution.

To improve the analysis of the functional data, we conducted further steps of the data preprocessing in FSL software using both FSL GUI and customised scripts. Imaging registration and distortion correction were performed by FEAT GUI (Smith *et al.*, 2004). The first stage of the neuroimaging preprocessing requires the removal of the skull tissue from the sMRI. In the LEMON study, MR2RAGE was acquired to improve the resolution. However, the canonical BET tool in FSL could not properly perform skull stripping due to the presence of the non-brain background signal. For these reasons, we took an alternative approach using a publicly available MATLAB script (Kashyap, 2021) to generate a clean T1-weighted image. We removed the first five volumes of the functional data for the signal stabilisation. Motion correction was performed with MCFLIRT, and geometric distortions were corrected using B0 with field map data (dwell time = 0.67 ms; unwarp direction = y-). Spatial smoothing, slice-timing correction were disabled as can be applied to resting state data (Kucikova *et al.*, 2023). Functional registration to subjects' high-resolution structural data was performed using

boundary-based registration (BBR; Greve and Fischl, 2009), after which nonlinear registration to the MNI standard space using FNIRT was applied. To remove physiological noise from the functional data, we applied independent component analysis (ICA; Beckmann *et al.*, 2005) using MELODIC to automatically identify noise components, which were removed using FMRIB’s ICA-based Xnoiseifier (FIX) with a trained classifier (Griffanti *et al.*, 2017). We adopted this approach based on previous studies that demonstrated its effectiveness in removing motion-related noise (Parkes *et al.*, 2018), which is important in group comparisons consisting of different ages. The denoised time series were band-pass filtered in the frequency range between 0.01 and 0.1 Hz. The temporal denoising step was applied outside of FSL in Nipype Python (adopting the code *Bandpass filtering: different outputs from FSL and nipype custom function - Neuro Questions*, 2017), as the results were different from the raw data (see **Figure 2.2**). To enable group-level analysis, all images were normalised to the MNI space with 2mm isotropic resolution.



**Figure 2.2.** Comparison of power spectral density (PSD) across different preprocessing approaches. The blue line represents the raw data, the green line shows data filtered using FSL’s default band-pass filtering, and the yellow line represents data filtered using a NumPy implementation.

The structural data was preprocessed with the FAST tool (FMRIB’s Automated Segmentation Tool; (Zhang, Brady and Smith, 2001), and included segmentation of T1-weighted images into grey matter, white matter, and cerebrospinal fluid (CSF), using bias field correction and spatial smoothing to improve the accuracy. Segmented images of different tissue types were normalised to the same MNI space as functional data.

After finishing functional and structural data preprocessing in FSL, we continued our analysis in the CONN toolbox to apply first-level and second-level analysis. After uploading the data, we visually inspected it and excluded it from the analysis one participant from Group 3 due to compromised structural data quality. Thus, there were 226 participants for further analysis. We also conducted a quality data control assessment and observed that some data were not normally distributed. To solve this issue, we additionally applied the regression of the CSF

signal. After this step, the quality control metrics showed that the data distribution was normalised. Functional connectivity was computed using ROI-to-ROI analysis in CONN with the application of a general linear model to assess connectivity in the predefined regions.

### 2.3 Graph theory analysis

According to the definition of the compensatory mechanism given in section 1.3, we use the degree centrality (DC) as a graph-theoretical measure to quantify group differences in functional connectivity. DC shows how many connections a brain region (node) has with other regions within a network. The CONN toolbox supports a group-level ROI-to-ROI analysis of this metric and other graph measures, such as global efficiency, local efficiency, clustering coefficient, and the characteristic path length. In CONN, these metrics are computed from unweighted, undirectional graphs, where nodes represent ROIs and edges correspond to functional connections that surpassed a threshold. The toolbox provides the Harvard-Oxford atlas with 132 ROIs as a default parcellation scheme. However, the number of regions of interest can considerably influence network properties, and an insufficient number of ROIs may lead to an underrepresentation of relationships between regions (Stanley *et al.*, 2013). We implemented the Brainnetome Atlas, which is a high-resolution, connectivity-based atlas with 210 cortical and 36 subcortical regions (Fan *et al.*, 2016). This atlas also allows correlating brain anatomy with psychological and cognitive functions. For each subject, a ROI-to-ROI adjacency matrix (RRC) was generated from denoised data, representing the level of functional connectivity between each pair of nodes. Each element is defined as the Fisher-transformed bivariate correlation coefficient between the BOLD time series of two ROIs, where each ROI's time series is the averaged signal of all voxels in this region (Nieto-Castanon, 2020).

RRC matrix was thresholded by using the concept of network cost (Cost), which is the proportion of the retained supra-thresholded connections to the total possible number of connections (Khazaei, Ebrahimzadeh and Babajani-Feremi, 2016). This value ranges from 0 (no connections) to 1 (a completely connected graph). Lower Cost values remove many edges, which may result in a disconnected graph, while higher Cost values keep weak connections that can make a graph denser with less significant connections. To determine an optimal threshold, we identify the maximised global cost efficiency (GCE), which is calculated as:

$$GCE = GE - Cost \quad (2.1)$$

$$GE = \frac{1}{N} \sum_{i \in N} GE_i = \frac{1}{N} \sum_{i \in N} \sum_{j \in N, j \neq i} \frac{1}{D_{ij}(N-1)} \quad (2.2)$$

Where  $GE$  is the overall global efficiency,  $GE_i$  is the global efficiency at a node  $i$ ,  $D$  is the shortest-path distance matrix, and  $N$  is the number of nodes in the graph.

We determined the optimal Cost value that maximises GCE (see **Equation (2.1)**) by evaluating GE for every subject and Cost values ranging from 0.05 to 0.31 with a step size of 0.01 (Behfar *et al.*, 2020). As can be seen in **Figure 2.3**, the optimal Cost was at 0.19, giving the highest GCE at approximately 0.37.

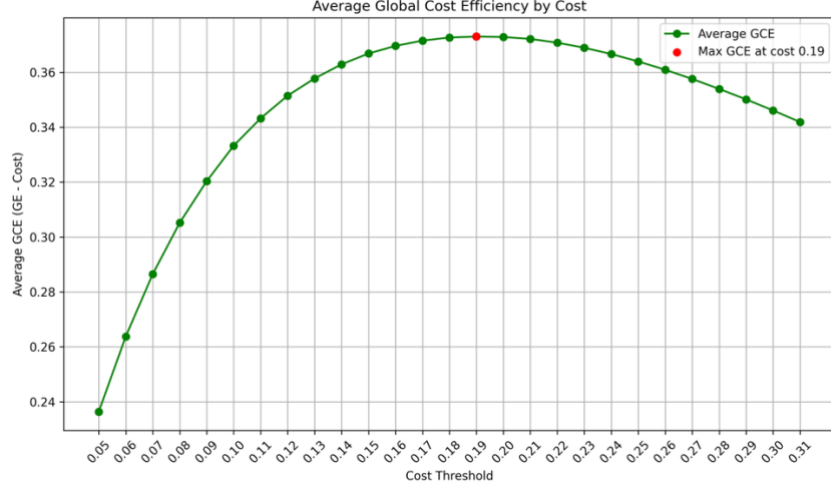


**Figure 2.3.** Average global cost efficiency (GCE) plotted against network cost (Cost) across all subjects. The green curve represents the mean GCE values, while the red dot indicates the Cost value at which the maximum GCE was achieved.

Subsequently, we applied this optimal value to the RRC matrix to ensure the balance between network density and efficiency.

Finally, we conducted the graph theory analysis at the group level. We exported the graph measures after conducting a between-group analysis on three groups of participants: younger adults (Group 1), early middle-aged adults (Group 2), and older adults (Group 3). The differences were determined using two-tailed t-tests with a  $p < 0.05$  (FDR-corrected) in three separate contrasts: Group 3 vs. Group 1, Group 3 vs. Group 2, and Group 1 vs. Group 2. DCs with significantly higher values were extracted for further correlation analysis with the performance on cognitive tests.

We applied the same steps to extract the values of global efficiency GE (as shown in **Equation (2.2)**), local efficiency LE (see **Equation (2.3)**), clustering coefficient CC (see **Equation (2.4)**), and average path length PL (**Equation (2.5)**). These metrics are defined in CONN (Nieto-Castanon, 2020) as:

$$LE_i = \frac{1}{d_i(d_i - 1)} \sum_{j \neq k, k \in \Gamma_i} \frac{1}{D_{jk}^{(i)}} \quad (2.3)$$

$$LE = \frac{1}{N} \sum_{i=1}^N LE_i$$

Where  $d$  represents a degree of each node,  $D$  denotes the shortest-path distance matrix within the local subgraph consisting of each node's  $i$  immediate neighbours  $j, k$  and the connections among them, and  $LE$  is the Local Efficiency of a graph.

The formulas for CC are:

$$CC_i = \frac{\sum_{j,k \in \Gamma_i} A_{j,k}^{(i)}}{d_i(d_i - 1)} \quad (2.4)$$

$$CC = \frac{1}{N} \sum_i CC_i$$

Where  $d$  denotes the degree of each node,  $A$  represents the adjacency matrix of the local subgraph formed by a node's  $i$  neighbours  $j, k$  and the connections among them, and  $CC$  is the clustering coefficient of a graph. The formulas for PL are:

$$PL_i = \frac{1}{N_i - 1} \sum_{j \in \Omega_i} D_{ij} \quad (2.5)$$

$$PL = \frac{1}{N} \sum_i L_i$$

Where  $D$  is the shortest-path distance matrix,  $N$  is the total number of nodes in a graph, and  $PL$  is the average path distance of a graph.

## 2.4 Grey Matter Volume Analysis

According to our hypothesis, a compensatory mechanism occurs when a region exhibits both increased functional connectivity and a reduction of grey matter (GM). Thus, we conducted a volumetric comparison of GM between different age groups. The preprocessing of T1-weighted images was conducted using FSL tools and custom bash scripts to prepare for the ROI-based morphometric analysis.

The brain-extracted GM images were segmented and normalised to the Montreal Neurological Institute (MNI) space. Subsequently, they were combined to create a group-average template. This template was smoothed using a Gaussian kernel with a 2 mm full-width at half-maximum (FWHM) to support the next step of nonlinear registration. Then, each individual's GM image was nonlinearly aligned to the smoothed group template using FNIRT (FMRIB's Non-linear Image Registration Tool). The warp fields generated during this registration were used to compute Jacobian determinant maps, which quantify local changes in the volume. These maps were applied to modulate the registered GM images, ensuring that the original tissue volumes were preserved. In the final step, the modulated images were smoothed

using an 8 mm FWHM Gaussian kernel to improve signal-to-noise ratio and account for anatomical differences across participants. GM volume was extracted for each ROI for further statistical analysis.

To assess GM volume differences among groups, we applied a general linear model for each ROI with the total intracranial volume (TIV) as a covariate to take into account differences in the brain size. TIV was calculated as the sum of the grey matter, white matter, and cerebrospinal fluid. To examine differences in the grey matter (GM) volume between age groups across brain regions, we ran a separate statistical test for each region of interest (ROI), taking into account differences in the brain size by including the total intracranial volume (TIV) as a covariate. For regions where GM volume followed a normal distribution, we used linear regression to model the GM volume based on age group and TIV. We then used ANOVA to test whether the age group had a significant effect. For regions where the GM data were not normally distributed, we first removed the effect of TIV by calculating residuals from a linear regression. We then compared these residuals between age groups using the Kruskal-Wallis test, a non-parametric method. We corrected all p-values for multiple comparisons using the false discovery rate (FDR) method. For regions showing significant group differences after correction, we did post-hoc tests to compare the older adults with each of the younger groups. These comparisons used independent t-tests (for normal regions) or Mann–Whitney U tests (for non-normal regions) on the TIV-corrected GM values. Only the regions where older adults had significantly lower GM volume than at least one younger group were included in the final summary and visualisation.

## 2.5 Cognitive Performance Correlation

To check our hypothesis on the compensatory effects in the ageing brain, we performed the final analysis step, where we investigated the relationship between the degree centrality (DC) in brain regions and cognitive performance, specifically within the older adults (Group 3).

During the acquisition of the data, multiple cognitive tests were conducted. The California Verbal Learning Task assesses verbal learning and memory. The Test of Attentional Performance measures different aspects of attention and working memory, including alertness, the ability to handle conflicting information, and short-term memory processing. The Trail Making Test evaluates cognitive flexibility, attention, and executive functioning. The Vocabulary Test assesses verbal intelligence and language comprehension. The Performance Testing System, Subtest 3, measures fluid intelligence. Lastly, the Regensburger Word Fluency Test measures verbal fluency. We examined correlations with all of the cognitive tests based

on the assumption that different brain regions exhibiting increased DC may be functionally related to different cognitive abilities.

DC values were extracted from RRC matrices at a cost threshold of 0.19 and z-scored across the subjects. The cognitive variable of interest was performance on a cognitive test, which was also z-scored. To control for potential confounding effects of age, as Group 3 included a wide range of ages (see **Figure 2.1**), we used multiple linear regression. For each ROI, a model was fitted with DC as the dependent variable and cognitive performance and age range as independent variables. To account for multiple comparisons across ROIs, we applied false discovery rate (FDR) correction to the resulting p-values. Only ROIs with FDR-corrected p-values below 0.05 were considered statistically significant.

## 3 Results

We analysed rs-fMRI, structural magnetic resonance imaging (sMRI) and cognitive test data from 226 participants. Participants were categorised into Group 1 (younger adults), Group 2 (early middle-aged adults), and Group 3 (older adults). Group comparisons were performed across these cohorts. In the following sections, comparisons between Group 1 and Group 2 are not discussed further, as no statistically significant differences were observed.

### 3.1 ROIs with a Significant Increase in DC between Groups

Second-level analyses were performed using the CONN toolbox to assess group differences between Group 3 vs. Group 1 and Group 3 vs. Group 2. Regions of interest (ROIs) were defined based on the Brainnetome Atlas. Their anatomical correspondence to Brodmann areas (BAs) is provided in **Appendix A**. Network-based statistics were employed, and the degree centrality (DC) was used as the primary graph-theoretical metric. Statistical results were thresholded at  $p < 0.05$  and FDR-corrected (two-sided) to account for multiple comparisons.

We observed an increase in DC in Group 3 compared to Group 1 in 43 ROIs (as seen in **Figure 3.1**, the left column). These regions are in the frontal lobe (23 ROIs), the parietal lobe (17 ROIs), two are in the limbic lobe, and one is in the occipital lobe. Most of these ROIs exhibited an increased DC in both left and right hemispheres. These bilateral ROIs are located in the precentral upper gyrus (PrG), specifically upper limb and trunk regions, the precentral lobule (PCL), in all lower limb regions, the middle frontal gyrus (MFG; BA *A9/46d*, *A46*, *A8vl*, and *A10l*), most regions of the superior parietal lobule (SPL; BA *A7r*, *A5l*, *A7pc*, and *A7ip*), the post central gyrus (PoG; upper limb, head and face regions, and trunk), and the precuneus (Pcun; BA *A5m*). The regions with increased DC that were located only in one of the hemispheres were the PrG (head and face region and BA *A6cdl* in the left hemisphere), the ventral part of the right MFG (BA *A9\_46v\_r*), the right superior frontal gyrus (SFG) in the medial areas (BA *A8m\_r* and *A9m\_r*) and dorsolateral area (BA *A6dl\_r*), the right inferior frontal gyrus (IFG; BA *A44op\_r*), the right caudal area of the inferior parietal lobule (IPL; BA *A40c\_r*) and the left rostradorsal area of the IPL (BA *A39rd\_l*), the caudal area of the SPL (BA *A7c*), the right caudal area (BA *A23c\_r*) and dorsal area (BA *A23d\_r*) of the cingulate gyrus (CG), and the right lateral occipital cortex (LOcC; BA *V5/MT\_plus*).

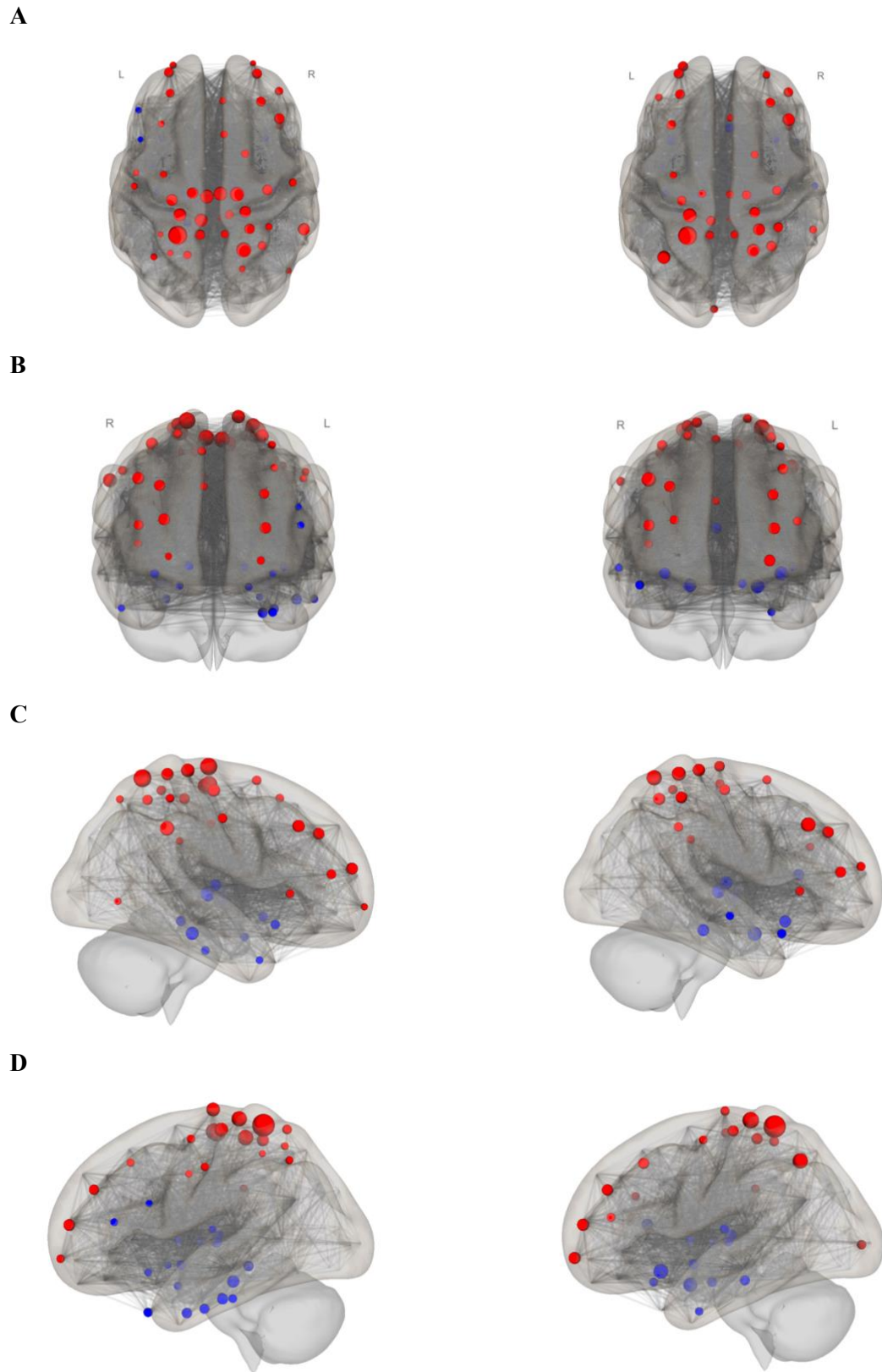


**Figure 3.1.** Group differences in the degree centrality (DC) visualised on the 3D brain models using the CONN toolbox. Each row presents a different view of the brain: superior (A), anterior (B), right lateral (C), and left lateral (D). The left column in each row shows regions with significant DC differences between Group 3 and Group 1, and the right column shows differences between Group 3 and Group 2. Red dots indicate regions of increased DC in Group 3 relative to the comparison group, while blue dots indicate decreased DC. Statistical results are based on the second-level general linear model (GLM) comparisons, with significance assessed using two-tailed tests and corrected for multiple comparisons using false discovery rate (FDR) correction at  $p < 0.05$ .

We also observed increased DC in Group 3 compared to Group 2 in 32 ROIs (as shown in **Figure 3.1**, the right column). These regions were distributed across the frontal lobe (18 ROIs), parietal lobe (11 ROIs), limbic lobe (2 ROIs), and occipital lobe (1 ROI). Most regions showed increased centrality bilaterally. These regions are located in the MFG (BA *A9/46d*, *A46*, *A9/46v*, and *A8vl*), the precentral upper gyrus (specifically upper limbs and trunk regions; BA *A4ul*, and *A4t*), the postcentral area of the SPL (BA *A7pc*), the trunk area of the PoG (BA *A1/2/3tru*), and the Pcun (BA *A5m*). Among the regions with increased DC that were lateralised to a single hemisphere were the lateral part of the left MFG (BA *A10l*), the PCL (lower limb regions; BA *A1/2/3ll\_l*, *A4ll\_r*), the right IFG (BA *A44op*), the right superior frontal gyrus in the dorsolateral area (BA *A6dl*), the caudal dorsolateral PrG (BA *A6cdl* in the left hemisphere), the right SPL of the rostral, lateral, and intraparietal areas (BA *A7r*, *A5l*, and *A7ip*), the right caudal area (BA *A40c*) and left rostradorsal (BA *A39rd*) areas of the IPL, the left caudal cuneus gyrus of the medio ventral occipital cortex (BA *cCunG*), and the right pregenual area (BA *A32p*) and dorsal area (BA *A23d*) of the cingulate gyrus.

### 3.2 ROI Morphometric Analysis of the Grey Matter

According to the hypothesis presented in Section 1.3, a key criterion for identifying a region of interest (ROI) as exhibiting compensatory mechanisms is the presence of increased degree centrality (DC) alongside the decreased grey matter volume. The ROI-based morphometry analysis, corrected for multiple comparisons using the false discovery rate (FDR), revealed 16 ROIs in the comparison between Group 3 and Group 1 that exhibited both increased DC and reduced GM volume. Similarly, 9 ROIs were identified in the comparison between Group 3 and Group 2. However, after adjusting for the total intracranial volume (TIV), these differences were no longer statistically significant in either GM volume or DC. ROIs that demonstrated GM reduction without a corresponding increase in DC are illustrated in **Figure 3.2**. Each violin plot shows the distribution of GM volume from a linear regression model with TIV as a covariate. In these ROIs, Group 3 displayed a significant decrease in GM compared to younger adults. Positive residuals indicate higher GM volume than expected based on TIV, while negative values indicate lower GM volume than expected.

We also examined whether GM volume correlates with the TIV across different age groups to account for the possibility that increases in cerebrospinal fluid (CSF) volume and decreases in GM and white matter (WM) volumes may occur while maintaining a relatively constant total brain volume (as shown in **Figure 3.3**).

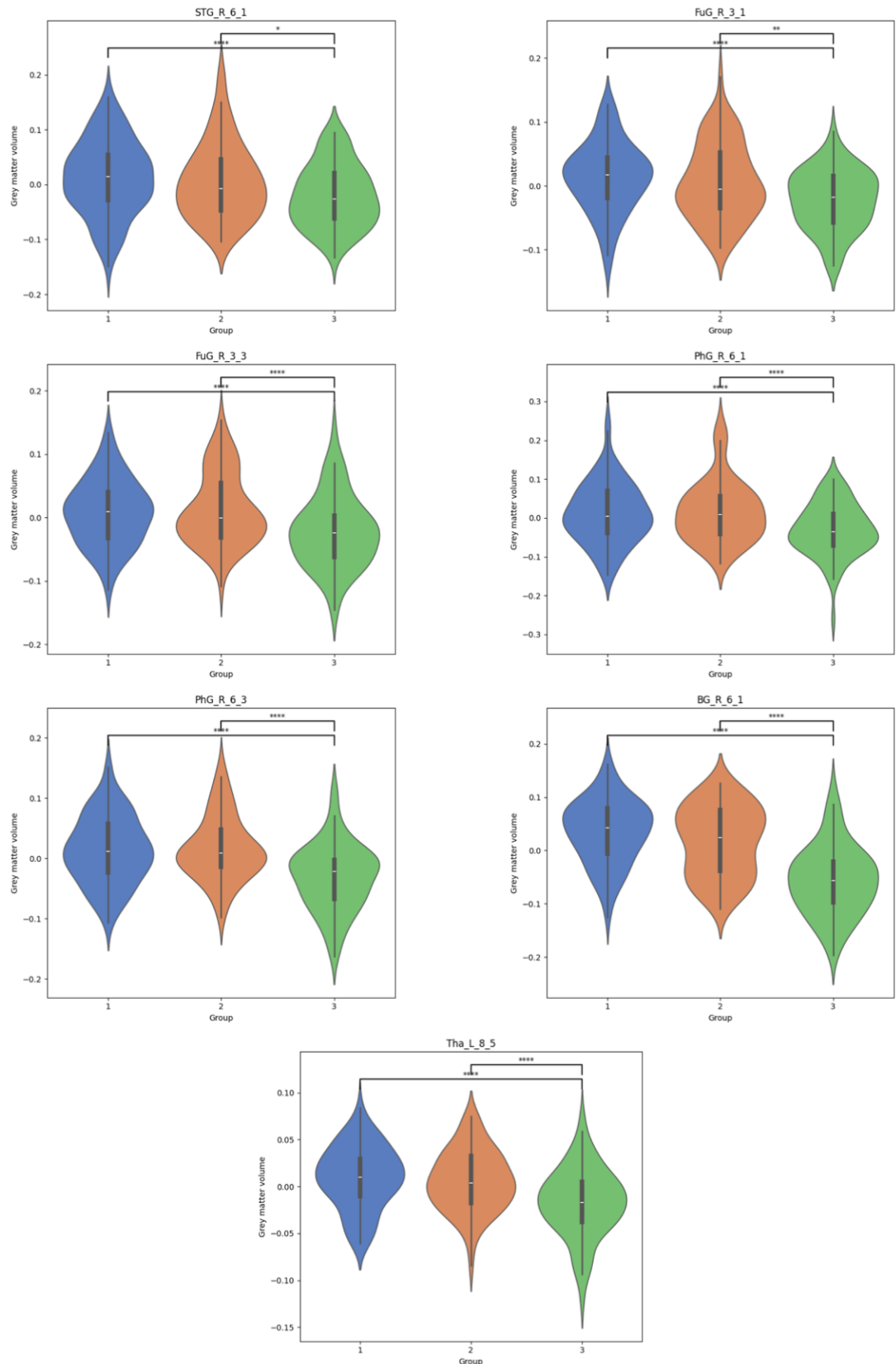


**Figure 3.2.** Grey matter volume differences in selected ROIs based on the Brainnetome Atlas. The figure illustrates grey matter volume across groups for: the medial area of the right superior temporal gyrus (STG\_R\_6\_1), the rostroventral and lateroventral areas of the right fusiform gyrus (FuG\_R\_3\_1 and FuG\_R\_3\_3), the rostral and posterior areas of the right parahippocampal gyrus (PhG\_R\_6\_1 and PhG\_R\_6\_3), the ventral caudal area of the right basal ganglia (BG\_R\_6\_1), and the left posterior parietal thalamus (Tha\_L\_8\_5). Statistical significance was assessed using ANCOVA with the total intracranial volume (TIV) as a covariate. Significance levels are denoted as follows:  $p < 0.05$  (\*),  $p < 0.01$  (\*\*),  $p < 0.005$  (\*\*\*), and  $p < 0.001$  (\*\*\*\*), all FDR-corrected.

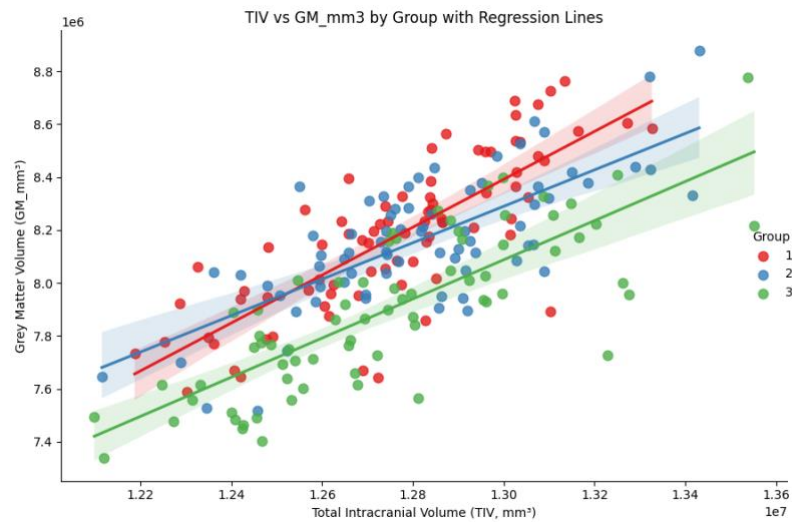


**Figure 3.3.** Grey matter (GM) volume as a function of total intracranial volume (TIV) across age groups. Regression lines are shown for younger (20–25, red), middle-aged (25–40, blue), and older adults (55–80, green) to assess whether age-related GM changes are independent of TIV.

The regions that showed a significant decrease in GM are the medial area of the right superior temporal gyrus (STG, BA *A38m*), the rostroventral and lateroventral areas of the right fusiform gyrus (FuG; BA *A20rv* and *A37lv*), the rostral area of the right parahippocampal gyrus (PhG; BA *A35/36r*), the right posterior parahippocampal gyrus (BA *TL*), the ventral caudal area of the right basal ganglia (BG; BA *vCa*), and the left posterior parietal thalamus (Tha; BA *Pptha*).

### 3.3 Correlation Analysis between ROIs with Increased DC and Cognitive Tests

We assessed all six cognitive tests administered during data acquisition, as ROIs with increased DC are known to support various cognitive functions, including working memory, attention, spatial processing, and reasoning. No significant correlations were observed after correcting for multiple comparisons, with one exception: performance on the Regensburger Wortflüssigkeitstest (RWT) significantly correlated with the DC of the right Parahippocampal Gyrus (as illustrated in **Figure 3.4**). The plot shows the relationship between degree centrality and the number of correctly produced S-words in RWT (both z-scored). A linear regression model controlling for different age distributions in Group 3 revealed a significant negative association ( $\beta = -0.44$ ,  $p = 0.033$ ), suggesting that lower verbal fluency was associated with higher centrality in this region. However, this region did not exhibit increased DC across the group comparisons and was therefore not included in the hypothesis-driven analysis.

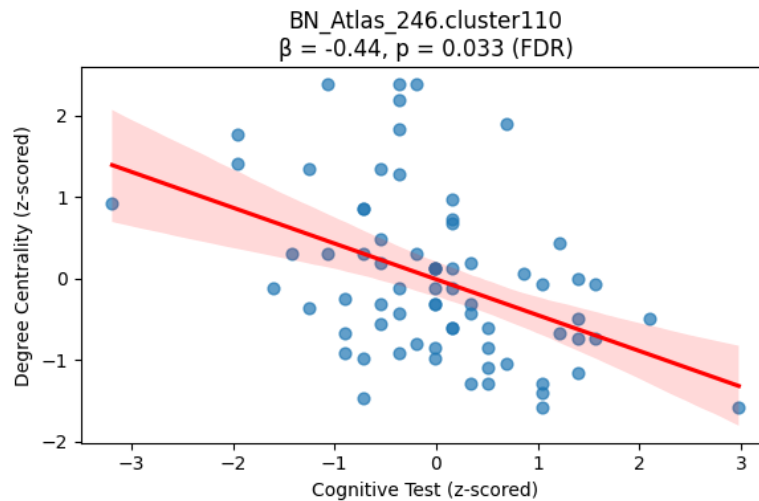


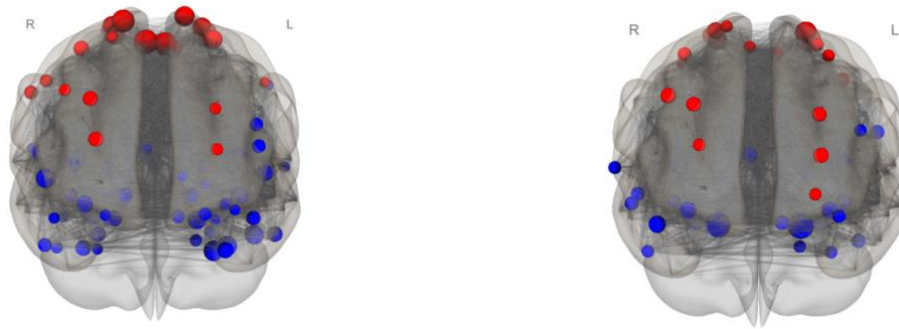
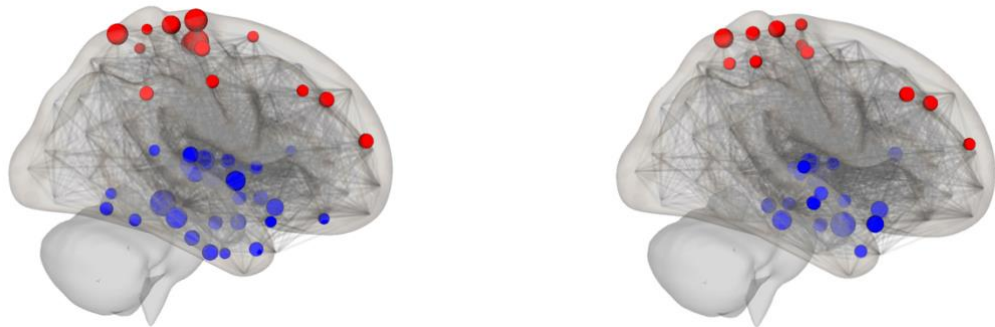
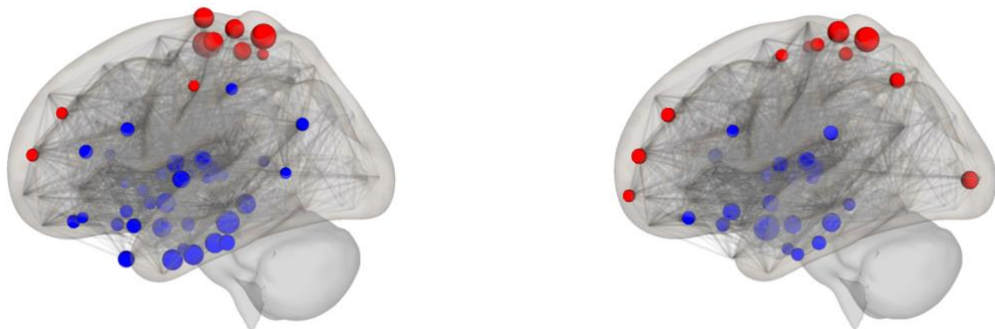
**Figure 3.4.** Correlation between degree centrality in the right Parahippocampal Gyrus (BN Atlas 246.cluster110) and verbal fluency in older adults (Group 3). Each dot represents one participant. The x-axis shows the z-scored number of correctly produced S-words in the Regensburger Wortflüssigkeitstest (RWT), and the y-axis shows z-scored degree centrality in this region. A linear regression model controlling for age revealed a significant negative association ( $\beta = -0.44$ ,  $p_{FDR} = 0.033$ ).

### 3.4 Global Efficiency, Local Efficiency, Clustering Coefficient, Characteristic Path Length, and Decreased Degree Centrality

All statistical tests reported below were corrected for multiple comparisons using the false discovery rate (FDR) method, with a significance threshold of  $p < 0.05$  (FDR-corrected, two-tailed).

Although the overall differences in the Global Efficiency (GE) between Group 3 and Group 1 or Group 2 were not statistically significant after correction for multiple comparisons, a considerable number of ROIs exhibited differences at the nodal level (**Appendix D**).

We identified 93 ROIs that showed differences in GE between Group 3 and Group 1 (see **Figure 3.5**, the left column). These regions were distributed across several brain lobes: 25 ROIs in the temporal lobe, all exhibiting a pronounced negative pattern; 12 ROIs in the parietal lobe, showing a marked positive tendency; 19 ROIs in the frontal lobe, mostly displaying a clear positive inclination except for the orbital gyrus, which showed a negative trend; 9 ROIs in the insular cortex, with a robust negative trend; 2 ROIs in the limbic lobe, both with a negative pattern; 21 ROIs in the subcortical nuclei, all exhibiting a consistently negative profile; and 1 ROI in the occipital lobe, which showed a negative trend. These regions included most areas of the bilateral parahippocampal gyri, fusiform gyri, superior and inferior temporal gyri, and somatomotor regions such as the lower limb, upper limb, and trunk representations of the paracentral lobules. Additional affected areas comprised the middle and inferior frontal gyri, the orbital gyri, the entire insular cortex, the majority of thalamic subregions, the amygdala, the basal ganglia, and the rostral portion of the hippocampus.

**A****B****C****D**

**Figure 3.5.** Group differences in the global efficiency (GE) visualised on 3D brain models using the CONN toolbox. Each row displays a different brain view: superior (A), anterior (B), right lateral (C), and left lateral (D). The left column in each row highlights regions with significant GE differences between Group 3 and Group 1, while the right column shows differences between Group 3 and Group 2. Red dots indicate regions where Group 3 shows increased GE relative to the comparison group, and blue dots indicate decreased efficiency. Statistical comparisons were performed using second-level general linear models (GLMs), with significance assessed using two-tailed tests and corrected for multiple comparisons via false discovery rate (FDR) correction at  $p < 0.05$ .

In the comparison between Group 3 and Group 2, GE differed significantly across 60 ROIs (**Figure 3.5**, the right column and **0**). These included 14 ROIs in the subcortical nuclei with a negative predominant trend, 9 ROIs in the parietal lobe, predominantly with positive trends except for the rostroventral inferior parietal lobule; 12 ROIs in the temporal lobe, all showing a clear negative inclination; and 15 ROIs in the frontal lobe, most of which exhibited a positive trend, with the exception of all areas of the orbital gyrus and the dorsal portion of the inferior frontal gyrus, which showed negative effects. Additionally, 8 ROIs in the insular lobe displayed a predominantly negative trend. Finally, the right rostroventral cingulate gyrus and the caudal cuneus of the medioventral occipital cortex showed a negative and a positive trend, respectively. These regions included bilateral amygdalae, multiple thalamic clusters, bilateral parahippocampal and hippocampal gyri, the basal ganglia, the cingulate gyrus, bilateral postcentral and precentral gyri, superior and inferior parietal lobules, and bilateral middle frontal gyri.

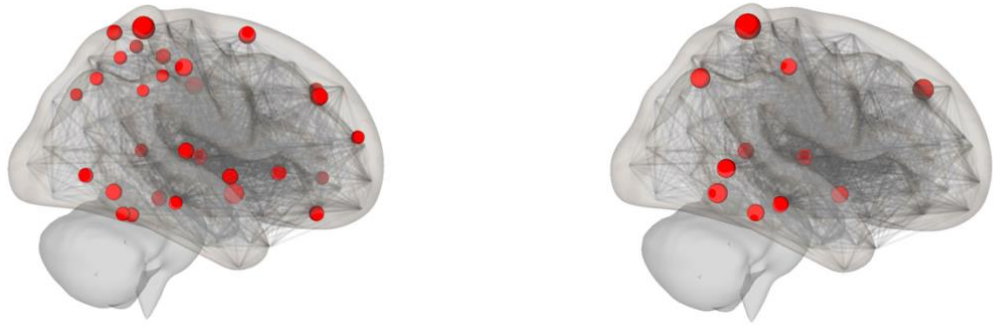
In the comparison between Group 3 and Group 1, the local efficiency (LE) was significantly increased across a broad set of brain regions (see **Figure 3.6**, the left column). The most prominent effects were found bilaterally in the insular cortex (7 ROIs) and in the parietal lobe (12 ROIs), including the superior and inferior parietal lobules, bilateral precuneus, and postcentral gyrus. Significant increases were also observed in the temporal lobe (10 ROIs), involving the fusiform gyrus, superior and inferior temporal gyri, and parahippocampal gyrus.

In the frontal lobe (9 ROIs), higher LE was found in the superior and middle frontal gyri as well as the orbital gyrus. Additional effects were present in the limbic lobe (4 ROIs), particularly in the cingulate gyrus, and in the occipital lobe (3 ROIs), specifically the lateral occipital cortex.

When assessing group differences between Group 3 and Group 2, the local efficiency (LE) was significantly increased in 14 cortical regions (as shown in **Figure 3.6**, the right column and shown in Error! Reference source not found.). The most pronounced effects were observed bilaterally in the parietal lobe, including the superior parietal lobule (SPL\_L\_5\_4, SPL\_R\_5\_4) and the right postcentral gyrus (PoG\_R\_4\_3). In the temporal lobe, significant increases were found in five regions, encompassing the inferior and middle temporal gyri (ITG\_L\_7\_6, ITG\_R\_7\_5, MTG\_R\_4\_3, MTG\_R\_4\_1). Additionally, elevated LE was detected in three regions of the insular cortex (INS\_L\_6\_4, INS\_R\_6\_4, INS\_R\_6\_1), the left superior frontal gyrus (SFG\_L\_7\_6), and the right cingulate gyrus (CG\_R\_7\_4).

We also examined differences in the clustering coefficient (CC) between Group 3 and Group 1. This comparison revealed a significant increase in CC across a wide range of brain regions, encompassing 52 ROIs (as seen in **Figure 3.7**, the left column and **Appendix H**).

A



B



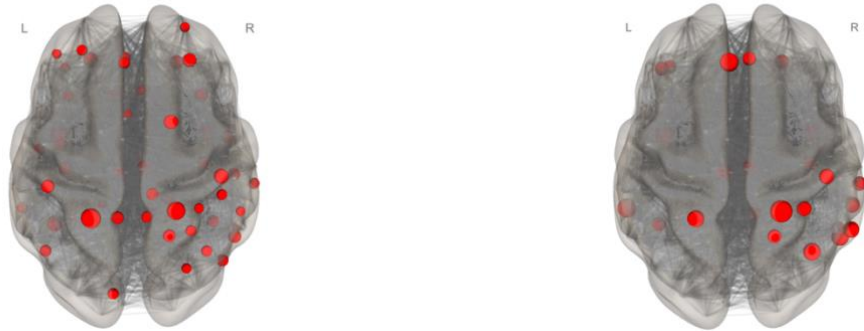
**Figure 3.6.** Group differences in the LE visualised on the 3D brain models using the CONN toolbox. Each row presents a different view of the brain: right lateral (A), and left lateral (B). The left column in each row shows regions with significant LE differences between Group 3 and Group 1, and the right column shows differences between Group 3 and Group 2. Red dots indicate regions of increased LE in Group 3 relative to the comparison group. Statistical results are based on second-level general linear model (GLM) comparisons, with significance assessed using two-tailed tests and corrected for multiple comparisons using false discovery rate correction at  $p < 0.05$ .

The most notable increases were observed bilaterally in the insular cortex (7 ROIs) and across the parietal lobe (13 ROIs), including the superior and inferior parietal lobules, the bilateral precuneus, and the postcentral gyrus. Significant elevations in CC were also detected in the temporal lobe (11 ROIs), involving the fusiform gyrus, superior, middle, and inferior temporal gyri, and the parahippocampal gyrus. In the frontal lobe (11 ROIs), higher CC values were identified in the orbital gyrus, as well as in the superior and middle frontal gyri. Additional regions showing increased CC included areas of the limbic lobe (6 ROIs), particularly the cingulate gyrus, the occipital lobe (3 ROIs), specifically the lateral occipital cortex, and the right thalamus.

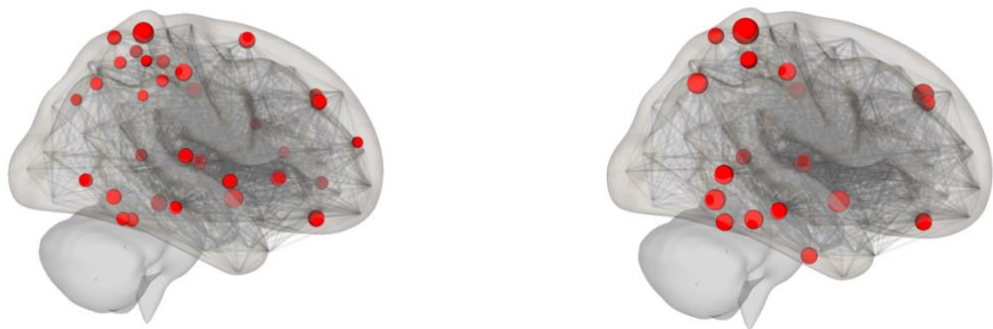
When comparing Group 3 to Group 1, the clustering coefficient (CC) was significantly elevated in 25 cortical regions (as seen in **Figure 3.7**, the right column and **Appendix I**). The most prominent changes appeared primarily unilaterally in the parietal lobe (6 ROIs), involving the superior and inferior parietal lobules as well as the right postcentral gyrus. In the temporal lobe, increases were observed in eight areas, including regions of the inferior and middle temporal gyri, and the fusiform gyrus. Higher CC values were also detected in three insular

regions, two regions of the superior frontal gyrus, three regions of the orbital gyrus, and three areas within the cingulate cortex.

A



B



C



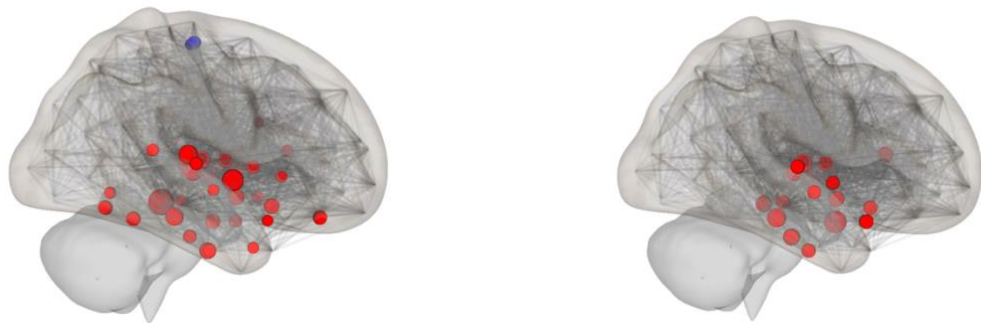
**Figure 3.7.** Group differences in CC visualised on 3D brain models using the CONN toolbox. Each row presents a different view of the brain: superior (A), right lateral (B), and left lateral (C). The left column in each row shows regions with significant CC differences between Group 3 and Group 1, and the right column shows differences between Group 3 and Group 2. Red dots indicate regions of increased CC in Group 3 relative to the comparison group. Statistical results are based on second-level general linear model (GLM) comparisons, with significance assessed using two-tailed tests and corrected for multiple comparisons using false discovery rate correction at  $p < 0.05$ .

The comparison of the characteristic path length (PL) between Group 3 and Group 1 revealed significant differences across 77 regions of interest (as illustrated in **Figure 3.8**, the left column and **Appendix J**). The majority of these regions exhibited positive beta values, indicating higher PL in Group 3 relative to Group 1. These increases were widespread, encompassing 22 subcortical ROIs, 27 ROIs within the temporal lobe, 12 in the insular cortex, 9 in the frontal lobe, 2 in the left inferior parietal lobule, 3 in the cingulate gyrus, as well as the right medio-ventral occipital cortex and the left lateral occipital cortex. In contrast, only three

regions showed a reduction in PL in Group 3: the left and right paracentral lobules and the left precentral gyrus.

We investigated differences in average pathway values between Group 3 and Group 2 (**Figure 3.8**, the right column and **Appendix K**). Several specific regions exhibited significant differences. The most pronounced increases were found in the left and right amygdala. In addition, elevated pathway values were observed in subcortical nuclei (8 ROIs), the temporal lobe (12 ROIs), and bilateral insular subregions (8 ROIs). Two regions within the orbital gyrus also showed significant increases, along with one region in the cingulate gyrus. Notably, only a single region – the left middle ventral occipital cortex – showed a significant decrease in pathway values.

A



B



**Figure 3.8.** Group differences in the characteristic path length (PL) visualised on 3D brain models using the CONN toolbox. Each row displays a different brain view: right lateral (A) and left lateral (B). The left column in each row highlights regions with significant PL differences between Group 3 and Group 1, while the right column shows differences between Group 3 and Group 2. Red dots indicate regions where Group 3 shows increased PL relative to the comparison group, and blue dots indicate decreased. Statistical comparisons were performed using second-level general linear models (GLMs), with significance assessed using two-tailed tests and corrected for multiple comparisons via false discovery rate (FDR) correction at  $p < 0.05$ .

## 4 Discussion

The primary aim of this study was to examine whether older adults exhibit compensatory mechanisms in functional brain networks by increasing functional connectivity in regions that show grey matter atrophy, while maintaining a positive association with cognitive performance. The criteria for identifying compensation were based on the framework proposed by Behfar *et al.* (2020), who explored this phenomenon in healthy ageing individuals and those with prodromal Alzheimer's disease. According to these criteria, a brain region is considered to reflect a compensatory mechanism if it shows (1) a significant increase in functional connectivity, measured using the graph-theoretical metric of degree centrality, and (2) a positive relationship with cognitive function. Additionally, these regions must simultaneously exhibit a decline in grey matter volume.

### 4.1 Interpretation of Key Findings

The graph-theoretical analysis of ROI-to-ROI connectivity matrices revealed several regions with increased degree centrality in both comparisons: older adults (N = 73, age range 55-80 years, median group is 65-70 years) vs. younger adults (N = 79, age range 20-25 years) and older adults vs. early middle-aged adults (N = 75, age range 25-40, median group is 25-30). The frontal lobe showed the highest concentration of such regions. Notably, the middle frontal gyrus demonstrated increased centrality and is functionally linked to social cognition, working memory, explicit memory, and reasoning, based on the BrainMap database (Fox and Lancaster, 2002; Fox *et al.*, 2005), which supports the functional annotation in the Brainnetome Atlas.

The left precentral gyrus, involved in action execution, speech production, shape discrimination, and spatial cognition, also showed increased degree centrality. Additional frontal regions with increased DC include the superior frontal gyrus, associated with working memory, attention, and action inhibition, and the inferior frontal gyrus, linked to time-related cognitive processes.

The parietal lobe also showed a substantial number of regions with increased DC in comparison with both younger groups, particularly in the superior parietal lobule and the precuneus. These areas are involved in a wide range of cognitive functions, including spatial cognition, attention, reasoning, action imagination, somatic processing, working memory, motion and colour perception, and social cognition.

Finally, in the limbic lobe, increased DC was detected in the cingulate gyrus compared to both younger groups, a region functionally associated with emotion, social cognition, explicit

memory, attention, and action inhibition. The medioventral occipital cortex, which also exhibited elevated degree centrality, is linked to semantic aspects of language processing.

This analysis allowed us to identify regions that meet the criteria for increased functional connectivity. Notably, the areas with the most prominent increases in degree centrality are functionally associated with action imagination and execution, bodily sensations, proprioception, motor learning, somatosensory processing, and pain perception. Furthermore, the comparison between older and younger adults revealed greater differences in regions linked to somatic functions such as bodily sensations and proprioception. In contrast, the comparison between older and early middle-aged adults showed more pronounced changes in areas related to both cognitive processes and somatic functions.

In the subsequent phase of our study, we conducted a comparison of GM volumes across age three groups. Previous research has consistently demonstrated that ageing is associated with reductions in both grey and white matter volumes, accompanied by an increase in cerebrospinal fluid volume (Podgórski *et al.*, 2021). This structural decline is a critical criterion in the definition of a compensatory mechanism, which is used in our study, where regions become more functionally interconnected even though they are structurally degrading, suggesting the compensatory adaptation of the brain.

The methodology chosen to assess GM volume loss significantly influences the detection of such changes. Voxel-based morphometry (VBM) offers a whole-brain, voxel-wise analysis capable of detecting brain tissue atrophy. In contrast, the ROI-based morphometry focuses on predefined areas, which may limit sensitivity (Seyedi *et al.*, 2020). Despite this limitation, we chose the ROI-based method because it allowed for a more straightforward comparison between structural and functional data in the same regions.

Our findings revealed significant GM volume reductions in several brain regions among older adults compared to younger groups. However, after adjusting for total intracranial volume (TIV), only specific areas maintained significant group differences: the right medial superior temporal gyrus, right rostroventral and lateroventral fusiform gyrus, right rostral and posterior parahippocampal gyrus, right ventral caudal basal ganglia, and left posterior parietal thalamus. All these regions are located in the right temporal lobe and lie in close proximity to one another. These regions are functionally associated with explicit memory, semantic and orthographic processing of words, emotional responses such as anger and fear, and the visual perception of shape. In older adults, they exhibited increased characteristic path length and decreased global efficiency, suggesting less efficient communication within the broader network, potentially because of the structural grey matter changes. However, the observed increases in local efficiency and clustering coefficient may reflect a compensatory reorganisation at the local

level, where neighbouring nodes become more interconnected to compensate for the reduced whole network efficiency.

Nevertheless, none of these regions showed increased degree centrality, which is a key criterion for identifying compensatory mechanisms in our study. As such, they do not meet the criteria to be considered as exhibiting compensatory effects in the ageing brain defined in the previous study. However, the results of the increased clustering coefficient and decreased GM volume in some particular regions might suggest the importance of considering compensation as not relying solely on the strength of a region's overall connectivity, but also on how well its neighbouring regions are interconnected.

On the other hand, the fact that the grey matter loss did not remain significant after adjusting for TIV may indicate that the structural changes associated with ageing are relatively subtle and not substantial enough compared to younger and early middle-aged adults. Healthy ageing, unlike neuropathological conditions such as traumatic brain injury, stroke, Alzheimer's disease, or Parkinson's disease, does not typically lead to severe deterioration of brain tissue.

In the final phase of our study, we explored whether any specific brain regions in older adults showed an increased number of functional connections (nodes) compared to other groups. We also examined whether such increases were associated with performance on a battery of cognitive tests. As suggested by the previous study, a compensatory mechanism in the ageing brain should be reflected in better cognitive performance.

Since the regions with increased degree centrality were functionally linked to domains such as explicit and working memory, language, and attention, we tested for associations with verbal learning, attention, cognitive flexibility, crystallised intelligence, and fluid intelligence. However, no significant correlations were found, except for a negative correlation between performance on the Regensburger Word Fluency Test and connectivity in the right rostral parahippocampal gyrus.

In this task, participants were asked to produce as many German words as possible beginning with the letter "S," serving as a measure of verbal fluency. Despite this finding, the right rostral parahippocampal gyrus did not show increased degree centrality and, therefore, did not meet our criteria for a compensatory region. Nonetheless, it is worth noting that this area did exhibit increased local connectivity.

Although the Brainnetome Atlas does not list behavioural associations for the right rostral parahippocampal gyrus, the left parahippocampal gyrus is functionally linked to explicit memory, semantic processing, and social cognition. While this is speculative, it raises the possibility that the right-hemisphere counterpart may play an analogous role.

It is important to note that Behfar *et al.* (2020) compared senior healthy controls and individuals diagnosed with mild cognitive impairment in their study. They also report the lack of significant correlations between the results of cognitive tests and functional connectivity in the control group, in contrast to the patient group. It can imply that in healthy ageing populations, cognitive test results may not exhibit a straightforward or linear relationship with functional connectivity, and the within-group differences, such as life experience and education level, may significantly affect the results in the ageing population. Conversely, patients with severe and profound neurological changes might exhibit clearer differences.

Overall, answering our research questions, we found the regions of interest in older adults that showed increased functional connectivity compared to younger adults. These regions are associated with diverse cognitive functions, but the correlation with performance in cognitive tests was not found. There was also no significant grey matter loss in those regions. These findings may suggest that the criteria used to define a compensatory mechanism may be more applicable to severe conditions such as neurodegenerative diseases, and may not adequately capture the more subtle changes that occur in the healthy ageing brain.

Further analysis of graph metrics was conducted to identify group differences in network topology. No significant differences were observed between the younger and early middle-aged groups. In contrast, extensive alterations in topological organisation were found in older adults, affecting multiple brain regions. However, these alterations were observed only at the regional level, as the network-level analyses did not reach significance after false discovery rate correction.

Temporal lobes bilaterally exhibited consistent patterns: reduced global efficiency and increased characteristic path length in all regions, showing significant changes. This pattern suggests a decline in integrative processing and long-range communication. Interestingly, these same regions showed increased local efficiency and clustering coefficient, indicating a potential compensatory mechanism at the level of local neighbourhoods.

Subcortical regions, however, demonstrated reduced global efficiency without concurrent increases in local efficiency or clustering, suggesting overall impaired communication both globally and locally.

In the insular lobe, all areas showed a decline in global communication simultaneously with increases in local efficiency and clustering in several regions. These regions are functionally associated with action inhibition, sensory experiences of the body that involve unpleasant feelings as a consequence of injuries, disease, or emotional disorders, the sense of tasting and the emotion of disgust. Yet, when comparing older adults with early middle-aged

individuals, only the ventral granular insular and hypergranular insular cortex showed significant increases at the local level.

Frontal regions displayed mixed patterns. The orbital gyrus and left inferior frontal gyrus showed reduced global efficiency and increased characteristic path lengths. These regions are implicated in emotional processing, particularly fear and sadness, as well as in gustatory perception, explicit memory, olfactory processing, and speech functions. Within the orbital gyrus, some areas also had increased neighbour clustering, but without a corresponding rise in local efficiency, except for the lateral orbital gyrus (Brodmann area A11). This suggests limited compensatory improvement in local information exchange. These regions are associated with gustation, emotion, and semantic processing. In contrast, regions such as the precentral gyrus, paracentral lobule, and middle frontal gyrus demonstrated increased global efficiency. The paracentral lobules and the precentral gyri related to action execution, action imagination, and motor learning demonstrated increased global efficiency. Moreover, the paracentral lobule enhanced local efficiency in the clusters. The superior and middle frontal gyri also showed enhanced local efficiency and neighbour clustering compared to younger adults, though these differences were not evident when compared to early middle-aged adults. Only the superior frontal gyrus showed increased neighbour interconnectivity in this latter comparison. These regions are associated with such cognitive functions as explicit and working memory, attention, reasoning, action inhibition, and social cognition.

In the parietal lobe, most areas showed increased global efficiency in older adults, with exceptions in specific subregions of the inferior parietal cortex (e.g., A39rv and A40rv), which did not follow this trend. Nevertheless, both areas with and without increased global efficiency demonstrated improvements in local efficiency and clustering. Functionally, they are associated with memory, reasoning, attention, spatial cognition, as well as perception of shape, action imagination and execution, speech execution, and somatic cognition.

Cingulate regions exhibited reduced global efficiency but enhanced local metrics, including both local efficiency and neighbour clustering, suggesting localised compensatory adaptations.

Contrary to typical findings in ageing studies, occipital regions did not show widespread decline. This observation is surprising in the context of the PASA (posterior-anterior shift in ageing) hypothesis, which describes a functional shift from posterior to frontal brain regions with age. Only the rostral lingual gyrus (medioventral occipital cortex) showed reduced global efficiency in older adults compared to younger ones. In contrast, the lateral occipital cortex exhibited increased local efficiency and neighbour clustering in older adults, and the left caudal cuneus gyrus showed elevated global efficiency. However, the medial superior occipital gyrus

demonstrated increased average path length, indicating reduced global integration in this region.

Overall, our findings suggest that ageing does not follow a uniform pattern of neural change across the entire brain. Instead, the data reveal a decline in global efficiency within the temporal lobes and subcortical regions, pointing to reduced capacity for information integration and exchange, and simultaneously, enhanced global and local efficiency in some regions of the frontal and parietal lobes. Notably, disruptions in subcortical structures such as the thalamus, basal ganglia, and amygdala may have consequent effects on cortical connectivity. In contrast, increased global and local efficiency in regions involved in emotional processing, motor execution, interoception, proprioception, memory, attention, and inhibitory control may reflect a compensatory response to subcortical deterioration. From the perspective of compensatory mechanisms, future research should examine the functional interplay between subcortical and cortical networks. ROI-based morphometry also indicated grey matter loss in the right ventral caudal basal ganglia, linked to cognition, emotion, and gustation, and in the left posterior parietal thalamus, associated with colour perception and motor function. These structural changes should be examined more closely in further investigation.

## 4.2 Limitations

Our study utilised an open-source dataset; hence, we had no control over the acquisition protocols. One of the most significant limitations is the distribution of age within the cohort. To address this, we divided the participants into three age groups (young, early middle-aged, and older adults) with approximately equal numbers in each group to preserve statistical power. However, the older adult group included a broad age range, from individuals in the late middle-age range (approximately 55–65 years) to those over 75 years. This heterogeneity may have introduced variability that could influence both functional and structural analyses. In addition, the sample was not well balanced in terms of gender, with a predominance of male participants in the younger and early middle-aged groups, which could also affect the results. This factor could also influence the absence of correlation between graph metrics and the performance on cognitive tests.

Another limitation concerns the use of an atlas-based region of interest (ROI) approach for both functional and structural analyses. While this method allows for direct comparison across modalities, it may lack the spatial resolution necessary to detect subtle group differences in the grey matter volume (Hayasaka and Laurienti, 2010). Future research should consider using voxel-based functional connectivity analyses to enable more precise comparisons between structural and functional data. Notably, the preprocessing pipeline applied here was

originally developed for voxel-wise functional connectivity, and this approach may be used in future studies.

The choice of the preprocessing pipeline and the sequence of steps can significantly influence the interpretation of the results, and it is an ongoing discussion among the neuroimaging research community on the usage of such approaches as global signal regression, which can distort group differences (Saad *et al.*, 2012).

The use of the CONN toolbox also introduced some methodological limitations. Specifically, it limited our functional connectivity analysis to ROI-to-ROI methods, as this is the only connectivity type within CONN that supports graph theory measures. Moreover, the toolbox restricts the range of available graph metrics and does not support the use of certain measures, such as the small-world index, which could provide additional insight into the network properties.

### 4.3 Future work

Due to limitations attributed to the use of the CONN toolbox, which allows only ROI-to-ROI graph-theoretical analysis, future work may benefit from applying voxel-to-voxel functional connectivity analysis followed by graph-theoretical characterisation. Taking into account the sensitivity of such analysis to the choice of parcellation schemes of the brain, it would be fruitful to compare the results of the topological properties of the brain in different ages, depending on the method of parcellation. While ROI-based approaches are commonly used in neuroimaging, voxel-wise analyses are less frequent due to their computational demands. However, investigating compensatory mechanisms in ageing and neuropathological conditions may require the higher resolution analysis of the data that the voxel-based approach can offer (McCarthy, Benuskova and Franz, 2014). This method can also improve the compatibility of different modality comparisons and allow the application of voxel-based morphometry, which can indicate subtle structural changes.

We also believe that the separation of the participants into high- and low-motion groups can increase the reliability of the functional connectivity analysis. In ageing research, motion-related noise is a significant concern, as it may produce spurious correlations in the data. Some studies report fewer age-related differences in graph metrics after accounting for motion (Kato *et al.*, 2020). This suggests that division into high and low motion groups may reveal more accurate findings.

Additionally, future research should examine connectivity between cortical and subcortical regions. Seed-to-ROI analysis can show how subcortical regions that displayed loss

of grey matter and a negative correlation with the cognitive test are correlated with the cortical regions.

Finally, while our current study is cross-sectional, such phenomena as compensatory mechanisms in the ageing brain require longitudinal designs that can reveal topological changes over time.

#### 4.4 Interdisciplinarity

This study is conducted in the field of cognitive neuroscience and implements computational approaches, including advanced neuroimaging data analysis and a machine learning algorithm for data preprocessing. By combining these methods, we aimed to establish the relationships between functional changes in the ageing brain and cognitive performance, linking neuroscience, computational methods, and cognitive psychology.

## 5 Conclusion

This research aimed to investigate whether older adults exhibit functional connectivity in particular regions compared to younger adults as a compensatory mechanism. To consider it as compensation, we asked several questions: whether these regions are associated with cognitive functions; whether these regions demonstrate a decrease in grey matter volume, and whether the increase in functional connectivity correlates with the performance on cognitive tests.

In the theoretical part of the thesis, we explored possible definitions of brain ageing and physiological characteristics that accompany this process. Brain ageing is a multifaceted phenomenon involving both localised and large-scale changes across different regions, which may in turn influence the overall network communication at both structural and functional levels. Cognitive ageing theories propose that with age, brain activity becomes less specialised, and compensatory mechanisms help maintain cognitive performance. Frameworks such as HAROLD, PASA, STAC, and cognitive reserve explain how the brain adapts through increased bilateral activity, a shift of activity toward frontal regions, reliance on supportive pathways, and sustained engagement in cognitive activity throughout life. We also considered methods that have been suggested as effective in studying these processes, such as structural and functional analysis. Thus, based on the theories described in the Introduction (see sections 1.1.3 and 1.2) and adopting the definition of compensatory mechanisms given by (Behfar *et al.*, 2020), we intended to analyse whether the brain regions with increased degree centrality in older adults compared to younger adults will also exhibit the loss of grey matter volume in the same regions and will correlate with the performance in cognitive tests.

We tested our assumptions by analysing graph-theoretical metrics across the three age groups. We applied general linear model analysis to resting-state fMRI data to examine functional connectivity between predefined regions of interest and compute connectivity matrices. We also applied the region-based morphometry of the structural MRI data to evaluate the grey matter loss in the regions with increased functional connectivity. To finalise our investigation, we explored the correlation between cognitive performance in psychological tests and the regions with increased degree centrality as a measure of connectivity of a node with the rest of the nodes. Finally, we compared other graph-theoretical metrics, such as the global efficiency, local efficiency, cluster coefficient, and average path length.

We found out that the older group displayed increased degree centrality in the frontal lobe and parietal lobe, which are associated with different cognitive functions such as attention, memory, spatial cognition, reasoning, and social cognition. Although we identified the loss of

grey matter in the temporal lobe and certain subcortical regions, we did not find a reduction in grey matter volume within the regions showing increased degree centrality, nor did we find significant correlations with cognitive test performance. Therefore, according to our definition, these findings did not support the presence of compensatory mechanisms in the regions with enhanced functional connectivity.

Our study showed that despite age-related changes in the topological properties of the functional brain organisation and structural alterations were observed, these changes do not fulfil the established criteria of compensatory mechanisms. The previous studies that applied these criteria and identified compensatory regions were conducted on clinical populations, which may be an important factor influencing their findings.

## 6 Bibliography

*Ageing and health* (no date). Available at: <https://www.who.int/news-room/fact-sheets/detail/ageing-and-health> (Accessed: 6 April 2024).

Ashburner, J. and Friston, K.J. (2000) ‘Voxel-Based Morphometry—The Methods’, *NeuroImage*, 11(6), pp. 805–821. Available at: <https://doi.org/10.1006/nimg.2000.0582>.

Aurich, N.K. *et al.* (2015) ‘Evaluating the reliability of different preprocessing steps to estimate graph theoretical measures in resting state fMRI data’, *Frontiers in Neuroscience*, 9, p. 48. Available at: <https://doi.org/10.3389/fnins.2015.00048>.

Babayan, A. *et al.* (2019) ‘A mind-brain-body dataset of MRI, EEG, cognition, emotion, and peripheral physiology in young and old adults’, *Scientific Data*, 6(1), p. 180308. Available at: <https://doi.org/10.1038/sdata.2018.308>.

*Bandpass filtering: different outputs from FSL and nipy custom function - Neuro Questions* (2017) *Neurostars*. Available at: <https://neurostars.org/t/bandpass-filtering-different-outputs-from-fsl-and-nipy-custom-function/824> (Accessed: 24 May 2025).

Beckmann, C.F. *et al.* (2005) ‘Investigations into resting-state connectivity using independent component analysis’, *Philosophical Transactions of the Royal Society of London. Series B, Biological Sciences*, 360(1457), pp. 1001–1013. Available at: <https://doi.org/10.1098/rstb.2005.1634>.

Behfar, Q. *et al.* (2020) ‘Graph Theory Analysis Reveals Resting-State Compensatory Mechanisms in Healthy Aging and Prodromal Alzheimer’s Disease’, *Frontiers in Aging Neuroscience*, 12. Available at: <https://doi.org/10.3389/fnagi.2020.576627>.

Bronikowski, A.M. (2010) ‘Aging and Its Demographic Measurement’.

Cabeza, R. (2002) ‘Hemispheric asymmetry reduction in older adults: the HAROLD model’, *Psychology and Aging*, 17(1), pp. 85–100. Available at: <https://doi.org/10.1037//0882-7974.17.1.85>.

Deery, H.A. *et al.* (2023) ‘The older adult brain is less modular, more integrated, and less efficient at rest: A systematic review of large-scale resting-state functional brain networks

in aging’, *Psychophysiology*, 60(1), p. e14159. Available at: <https://doi.org/10.1111/psyp.14159>.

Erol, A. and Hunyadi, B. (2022) ‘Chapter 12 - Tensors for neuroimaging: A review on applications of tensors to unravel the mysteries of the brain’, in Y. Liu (ed.) *Tensors for Data Processing*. Academic Press, pp. 427–482. Available at: <https://doi.org/10.1016/B978-0-12-824447-0.00018-2>.

Fan, L. *et al.* (2016) ‘The Human Brainnetome Atlas: A New Brain Atlas Based on Connectional Architecture’, *Cerebral Cortex (New York, NY)*, 26(8), pp. 3508–3526. Available at: <https://doi.org/10.1093/cercor/bhw157>.

Farahani, F.V., Karwowski, W. and Lighthall, N.R. (2019) ‘Application of Graph Theory for Identifying Connectivity Patterns in Human Brain Networks: A Systematic Review’, *Frontiers in Neuroscience*, 13. Available at: <https://www.frontiersin.org/journals/neuroscience/articles/10.3389/fnins.2019.00585> (Accessed: 21 February 2024).

Fox, P.T. *et al.* (2005) ‘Brainmap taxonomy of experimental design: Description and evaluation’, *Human Brain Mapping*, 25(1), pp. 185–198. Available at: <https://doi.org/10.1002/hbm.20141>.

Fox, P.T. and Lancaster, J.L. (2002) ‘Mapping context and content: the BrainMap model’, *Nature Reviews Neuroscience*, 3(4), pp. 319–321. Available at: <https://doi.org/10.1038/nrn789>.

Friston, K.J. (2011) ‘Functional and Effective Connectivity: A Review’, *Brain Connectivity*, 1(1), pp. 13–36. Available at: <https://doi.org/10.1089/brain.2011.0008>.

Gaspar-Silva, F., Trigo, D. and Magalhaes, J. (2023) ‘Ageing in the brain: mechanisms and rejuvenating strategies’, *Cellular and Molecular Life Sciences*, 80(7), p. 190. Available at: <https://doi.org/10.1007/s00018-023-04832-6>.

Giorgio, A. *et al.* (2010) ‘Age-related changes in grey and white matter structure throughout adulthood’, *NeuroImage*, 51(3), pp. 943–951. Available at: <https://doi.org/10.1016/j.neuroimage.2010.03.004>.

Greve, D.N. and Fischl, B. (2009) 'Accurate and robust brain image alignment using boundary-based registration', *NeuroImage*, 48(1), pp. 63–72. Available at: <https://doi.org/10.1016/j.neuroimage.2009.06.060>.

Griffanti, L. *et al.* (2017) 'Hand classification of fMRI ICA noise components', *NeuroImage*, 154, pp. 188–205. Available at: <https://doi.org/10.1016/j.neuroimage.2016.12.036>.

Hayasaka, S. and Laurienti, P.J. (2010) 'Comparison of characteristics between region- and voxel-based network analyses in resting-state fMRI data', *NeuroImage*, 50(2), pp. 499–508. Available at: <https://doi.org/10.1016/j.neuroimage.2009.12.051>.

Hülür, G. *et al.* (2015) 'Cognitive dedifferentiation with increasing age and proximity of death: Within-person evidence from the Seattle Longitudinal Study.', *Psychology and Aging*, 30(2), pp. 311–323. Available at: <https://doi.org/10.1037/a0039260>.

Jenkinson, M. *et al.* (2012) 'FSL', *NeuroImage*, 62(2), pp. 782–790. Available at: <https://doi.org/10.1016/j.neuroimage.2011.09.015>.

Jones, D.K. (2010) 'Challenges and limitations of quantifying brain connectivity *in vivo* with diffusion MRI', *Imaging in Medicine*, 2(3), pp. 341–355. Available at: <https://doi.org/10.2217/iim.10.21>.

Karaarslan, E. and Arslan, A. (2008) 'Diffusion weighted MR imaging in non-infarct lesions of the brain', *European Journal of Radiology*, 65(3), pp. 402–416. Available at: <https://doi.org/10.1016/j.ejrad.2007.04.023>.

Kashyap, S. (2021) 'srikash/presurfer: ondu'. Zenodo. Available at: <https://doi.org/10.5281/zenodo.4626841>.

Kato, S. *et al.* (2020) 'Effects of Head Motion on the Evaluation of Age-related Brain Network Changes Using Resting State Functional MRI', *Magnetic Resonance in Medical Sciences*, 20(4), pp. 338–346. Available at: <https://doi.org/10.2463/mrms.mp.2020-0081>.

Khazae, A., Ebrahimzadeh, A. and Babajani-Feremi, A. (2016) 'Application of advanced machine learning methods on resting-state fMRI network for identification of mild cognitive impairment and Alzheimer's disease', *Brain Imaging and Behavior*, 10(3), pp. 799–817. Available at: <https://doi.org/10.1007/s11682-015-9448-7>.

Kucikova, L. *et al.* (2023) ‘Computational Modeling of Neural Networks of the Human Brain’, in P. Vlamos, I.S. Kotsireas, and I. Tarnanas (eds) *Handbook of Computational Neurodegeneration*. Cham: Springer International Publishing, pp. 11–30. Available at: [https://doi.org/10.1007/978-3-319-75922-7\\_63](https://doi.org/10.1007/978-3-319-75922-7_63).

Kurth, F., Luders, E. and Gaser, C. (2015) ‘Voxel-Based Morphometry’, in *Brain Mapping*. Elsevier, pp. 345–349. Available at: <https://doi.org/10.1016/B978-0-12-397025-1.00304-3>.

Li, Q. *et al.* (2020) ‘Longitudinal Changes in Whole-Brain Functional Connectivity Strength Patterns and the Relationship With the Global Cognitive Decline in Older Adults’, *Frontiers in Aging Neuroscience*, 12. Available at: <https://doi.org/10.3389/fnagi.2020.00071>.

López-Otín, C. *et al.* (2023) ‘Hallmarks of aging: An expanding universe’, *Cell*, 186(2), pp. 243–278. Available at: <https://doi.org/10.1016/j.cell.2022.11.001>.

McCarthy, P., Benuskova, L. and Franz, E.A. (2014) ‘The age-related posterior-anterior shift as revealed by voxelwise analysis of functional brain networks’, *Frontiers in Aging Neuroscience*, 6. Available at: <https://doi.org/10.3389/fnagi.2014.00301>.

Milano, M., Guzzi, P.H. and Cannataro, M. (2019) ‘Network building and analysis in connectomics studies: a review of algorithms, databases and technologies’, *Network Modeling Analysis in Health Informatics and Bioinformatics*, 8(1), pp. 1–16. Available at: <https://doi.org/10.1007/s13721-019-0192-6>.

*MPI-Leipzig\_Mind-Brain-Body - OpenNeuro* (no date). Available at: <https://openneuro.org/datasets/ds000221/versions/00002> (Accessed: 21 April 2025).

Murman, D.L. (2015) ‘The Impact of Age on Cognition’, *Seminars in Hearing*, 36(3), pp. 111–121. Available at: <https://doi.org/10.1055/s-0035-1555115>.

Nieto-Castanon, A. (2020) *Handbook of functional connectivity Magnetic Resonance Imaging methods in CONN*. Hilbert Press. Available at: <https://doi.org/10.56441/hilbertpress.2207.6598>.

Nieto-Castanon, A. and Whitfield-Gabrieli, S. (2022) *CONN functional connectivity toolbox: RRID SCR\_009550, release 22*. 22nd edn. Hilbert Press. Available at: <https://doi.org/10.56441/hilbertpress.2246.5840>.

Oschmann, M. and Gawryluk, J.R. (2020) ‘A Longitudinal Study of Changes in Resting-State Functional Magnetic Resonance Imaging Functional Connectivity Networks During Healthy Aging’, *Brain Connectivity*, 10(7), pp. 377–384. Available at: <https://doi.org/10.1089/brain.2019.0724>.

Parkes, L. *et al.* (2018) ‘An evaluation of the efficacy, reliability, and sensitivity of motion correction strategies for resting-state functional MRI’, *NeuroImage*, 171, pp. 415–436. Available at: <https://doi.org/10.1016/j.neuroimage.2017.12.073>.

Podgórski, P. *et al.* (2021) ‘Novel Volumetric and Surface-Based Magnetic Resonance Indices of the Aging Brain – Does Male and Female Brain Age in the Same Way?’, *Frontiers in Neurology*, 12, p. 645729. Available at: <https://doi.org/10.3389/fneur.2021.645729>.

Ramanoël, S. *et al.* (2018) ‘Gray Matter Volume and Cognitive Performance During Normal Aging. A Voxel-Based Morphometry Study’, *Frontiers in Aging Neuroscience*, 10, p. 235. Available at: <https://doi.org/10.3389/fnagi.2018.00235>.

Reuter-Lorenz, P.A. and Cappell, K.A. (2008) ‘Neurocognitive Aging and the Compensation Hypothesis’, *Current Directions in Psychological Science*, 17(3), pp. 177–182. Available at: <https://doi.org/10.1111/j.1467-8721.2008.00570.x>.

Reuter-Lorenz, P.A. and Park, D.C. (2014) ‘How Does it STAC Up? Revisiting the Scaffolding Theory of Aging and Cognition’, *Neuropsychology Review*, 24(3), pp. 355–370. Available at: <https://doi.org/10.1007/s11065-014-9270-9>.

Rose, M. *et al.* (2012) ‘What is Aging?’, *Frontiers in Genetics*, 3. Available at: <https://doi.org/10.3389/fgene.2012.00134>.

Rubinov, M. and Sporns, O. (2010) ‘Complex network measures of brain connectivity: Uses and interpretations’, *NeuroImage*, 52(3), pp. 1059–1069. Available at: <https://doi.org/10.1016/j.neuroimage.2009.10.003>.

Saad, Z.S. *et al.* (2012) ‘Trouble at Rest: How Correlation Patterns and Group Differences Become Distorted After Global Signal Regression’, *Brain Connectivity*, 2(1), pp. 25–32. Available at: <https://doi.org/10.1089/brain.2012.0080>.

Sala-Llonch, R., Bartrés-Faz, D. and Junqué, C. (2015) ‘Reorganization of brain networks in aging: a review of functional connectivity studies’, *Frontiers in Psychology*, 6. Available at: <https://doi.org/10.3389/fpsyg.2015.00663>.

Seyedi, S. *et al.* (2020) ‘Comparing VBM and ROI analyses for detection of gray matter abnormalities in patients with bipolar disorder using MRI’, *Middle East Current Psychiatry*, 27(1), p. 69. Available at: <https://doi.org/10.1186/s43045-020-00076-3>.

Smith, S.M. *et al.* (2004) ‘Advances in functional and structural MR image analysis and implementation as FSL’, *NeuroImage*, 23, pp. S208–S219. Available at: <https://doi.org/10.1016/j.neuroimage.2004.07.051>.

Sporns, O. (2018) ‘Graph theory methods: applications in brain networks’, *Dialogues in Clinical Neuroscience*, 20(2), pp. 111–121. Available at: <https://doi.org/10.31887/DCNS.2018.20.2/osporns>.

Stanley, M.L. *et al.* (2013) ‘Defining nodes in complex brain networks’, *Frontiers in Computational Neuroscience*, 7. Available at: <https://doi.org/10.3389/fncom.2013.00169>.

Stern, Y. (2012) ‘Cognitive reserve in ageing and Alzheimer’s disease’, *The Lancet Neurology*, 11(11), pp. 1006–1012. Available at: [https://doi.org/10.1016/S1474-4422\(12\)70191-6](https://doi.org/10.1016/S1474-4422(12)70191-6).

Tanglay, O. *et al.* (2023) ‘Graph Theory Measures and Their Application to Neurosurgical Eloquence’, *Cancers*, 15(2), p. 556. Available at: <https://doi.org/10.3390/cancers15020556>.

Tognoli, E. and Kelso, J.A.S. (2014) ‘The Metastable Brain’, *Neuron*, 81(1), pp. 35–48. Available at: <https://doi.org/10.1016/j.neuron.2013.12.022>.

Varangis Burns, E.M., Habeck, C.G. and Stern, Y. (2020) ‘Task-based functional connectivity in aging: How task and connectivity methodology affect discovery of age effects’, 11(1). Available at: <https://doi.org/10.7916/d8-3tc8-7z78>.

Westlye, L.T. *et al.* (2010) ‘Life-Span Changes of the Human Brain White Matter: Diffusion Tensor Imaging (DTI) and Volumetry’, *Cerebral Cortex*, 20(9), pp. 2055–2068. Available at: <https://doi.org/10.1093/cercor/bhp280>.

Zhang, Y., Brady, M. and Smith, S. (2001) ‘Segmentation of brain MR images through a hidden Markov random field model and the expectation-maximization algorithm’, *IEEE Transactions on Medical Imaging*, 20(1), pp. 45–57. Available at: <https://doi.org/10.1109/42.906424>.

Zonneveld, H.I. *et al.* (2019) 'Patterns of functional connectivity in an aging population: The Rotterdam Study', *NeuroImage*, 189, pp. 432–444. Available at: <https://doi.org/10.1016/j.neuroimage.2019.01.041>.

## Appendix A Brainnetome Atlas Subregions Table

Lobe	Gyrus	Left and Right Hemisphere	Label ID.L	Label ID.R	Anatomical and modified Cyto-architectonic descriptions	lh.MNI (X,Y,Z)	rh.MNI (X,Y,Z)
Frontal Lobe	SFG, Superior Frontal Gyrus	SFG_L(R)_7_1	1	2	A8m, medial area 8	-5, 15, 54	7, 16, 54
		SFG_L(R)_7_2	3	4	A8dl, dorsolateral area 8	-18, 24, 53	22, 26, 51
		SFG_L(R)_7_3	5	6	A9l, lateral area 9	-11, 49, 40	13, 48, 40
		SFG_L(R)_7_4	7	8	A6dl, dorsolateral area 6	-18, -1, 65	20, 4, 64
		SFG_L(R)_7_5	9	10	A6m, medial area 6	-6, -5, 58	7, -4, 60
		SFG_L(R)_7_6	11	12	A9m,medial area 9	-5, 36, 38	6, 38, 35
		SFG_L(R)_7_7	13	14	A10m, medial area 10	-8, 56, 15	8, 58, 13
	MFG, Middle Frontal Gyrus	MFG_L(R)_7_1	15	16	A9/46d, dorsal area 9/46	-27, 43, 31	30, 37, 36
		MFG_L(R)_7_2	17	18	IFJ, inferior frontal junction	-42, 13, 36	42, 11, 39
		MFG_L(R)_7_3	19	20	A46, area 46	-28, 56, 12	28, 55, 17
		MFG_L(R)_7_4	21	22	A9/46v, ventral area 9/46	-41, 41, 16	42, 44, 14
		MFG_L(R)_7_5	23	24	A8vl, ventrolateral area 8	-33, 23, 45	42, 27, 39
		MFG_L(R)_7_6	25	26	A6vl, ventrolateral area 6	-32, 4, 55	34, 8, 54
		MFG_L(R)_7_7	27	28	A10l, lateral area10	-26, 60, -6	25, 61, -4
	IFG, Inferior Frontal Gyrus	IFG_L(R)_6_1	29	30	A44d,dorsal area 44	-46, 13, 24	45, 16, 25
		IFG_L(R)_6_2	31	32	IFS, inferior frontal sulcus	-47, 32, 14	48, 35, 13
		IFG_L(R)_6_3	33	34	A45c, caudal area 45	-53, 23, 11	54, 24, 12
		IFG_L(R)_6_4	35	36	A45r, rostral area 45	-49, 36, -3	51, 36, -1
		IFG_L(R)_6_5	37	38	A44op, opercular area 44	-39, 23, 4	42, 22, 3
		IFG_L(R)_6_6	39	40	A44v, ventral area 44	-52, 13, 6	54, 14, 11

	OrG, Orbital Gyrus	OrG_L(R)_6_1	41	42	A14m, medial area 14	-7, 54, -7	6, 47, -7	
		OrG_L(R)_6_2	43	44	A12/47o, orbital area 12/47	-36, 33, 16	40, 39, -14	
		OrG_L(R)_6_3	45	46	A11l, lateral area 11	-23, 38, 18	23, 36, -18	
		OrG_L(R)_6_4	47	48	A11m, medial area 11	-6, 52, 19	6, 57, -16	
		OrG_L(R)_6_5	49	50	A13, area 13	-10, 18, 19	9, 20, -19	
		OrG_L(R)_6_6	51	52	A12/47l, lateral area 12/47	-41, 32, -9	42, 31, -9	
	PrG, Precentral Gyrus	PrG_L(R)_6_1	53	54	A4hf, area 4(head and face region)	-49, 8, 39	55, -2, 33	
		PrG_L(R)_6_2	55	56	A6cdl, caudal dorsolateral area 6	-32, 9, 58	33, -7, 57	
		PrG_L(R)_6_3	57	58	A4ul, area 4(upper limb region)	-26, 25, 63	34, -19, 59	
		PrG_L(R)_6_4	59	60	A4t, area 4(trunk region)	-13, 20, 73	15, -22, 71	
		PrG_L(R)_6_5	61	62	A4tl, area 4(tongue and larynx region)	-52, 0, 8	54, 4, 9	
		PrG_L(R)_6_6	63	64	A6cvl, caudal ventrolateral area 6	-49, 5, 30	51, 7, 30	
	PCL, Paracentral Lobule	PCL_L(R)_2_1	65	66	A1/2/3ll, area1/2/3 (lower limb region)	-8, 38, 58	10, -34, 54	
		PCL_L(R)_2_2	67	68	A4ll, area 4, (lower limb region)	-4, 23, 61	5, -21, 61	
	Temporal Lobe	STG, Superior Temporal Gyrus	STG_L(R)_6_1	69	70	A38m, medial area 38	-32, 14, 34	31, 15, -34
			STG_L(R)_6_2	71	72	A41/42, area 41/42	-54, 32, 12	54, -24, 11
			STG_L(R)_6_3	73	74	TE1.0 and TE1.2	-50, 11, 1	51, -4, -1
			STG_L(R)_6_4	75	76	A22c, caudal area 22	-62, 33, 7	66, -20, 6
STG_L(R)_6_5			77	78	A38l, lateral area 38	-45, 11, 20	47, 12, -20	
STG_L(R)_6_6			79	80	A22r, rostral area 22	-55, 3, -10	56, -12, -5	
MTG, Middle Temporal Gyrus		MTG_L(R)_4_1	81	82	A21c, caudal area 21	-65, 30, 12	65, -29, -13	
		MTG_L(R)_4_2	83	84	A21r, rostral area 21	-53, 2, -30	51, 6, -32	
		MTG_L(R)_4_3	85	86	A37dl, dorsolateral area37	-59, 58, 4	60, -53, 3	
		MTG_L(R)_4_4	87	88	aSTS, anterior superior temporal sulcus	-58, 20, -9	58, -16, -10	

	ITG, Inferior Temporal Gyrus	ITG_L(R)_7_1	89	90	A20iv, intermediate ventral area 20	-45, - 26, - 27	46, - 14, - 33	
		ITG_L(R)_7_2	91	92	A37elv, extreme lateroventral area37	-51, - 57, - 15	53, - 52, - 18	
		ITG_L(R)_7_3	93	94	A20r, rostral area 20	-43, - 2, -41	40, 0, -43	
		ITG_L(R)_7_4	95	96	A20il, intermediate lateral area 20	-56, - 16, - 28	55, - 11, - 32	
		ITG_L(R)_7_5	97	98	A37vl, ventrolateral area 37	-55, - 60, -6	54, - 57, -8	
		ITG_L(R)_7_6	99	100	A20cl, caudolateral of area 20	-59, - 42, - 16	61, - 40, - 17	
		ITG_L(R)_7_7	101	102	A20cv, caudoventral of area 20	-55, - 31, - 27	54, - 31, - 26	
	FuG, Fusiform Gyrus	FuG_L(R)_3_1	103	104	A20rv, rostroventral area 20	-33, - 16, - 32	33, - 15, - 34	
		FuG_L(R)_3_2	105	106	A37mv, medioventral area37	-31, - 64, - 14	31, - 62, - 14	
		FuG_L(R)_3_3	107	108	A37lv, lateroventral area37	-42, - 51, - 17	43, - 49, - 19	
	PhG, Parahippoc ampal Gyrus	PhG_L(R)_6_1	109	110	A35/36r, rostral area 35/36	-27, - 7, -34	28, -8, -33	
		PhG_L(R)_6_2	111	112	A35/36c, caudal area 35/36	-25, - 25, - 26	26, - 23, - 27	
		PhG_L(R)_6_3	113	114	TL, area TL (lateral PPHC, posterior parahippocampal gyrus)	-28, - 32, - 18	30, - 30, - 18	
		PhG_L(R)_6_4	115	116	A28/34, area 28/34 (EC, entorhinal cortex)	-19, - 12, - 30	19, - 10, - 30	
		PhG_L(R)_6_5	117	118	TI, area TI(temporal agranular insular cortex)	-23, - 2, -32	22, 1, -36	
		PhG_L(R)_6_6	119	120	TH, area TH (medial PPHC)	-17, - 39, - 10	19, - 36, - 11	
	pSTS, posterior Superior Temporal Sulcus	pSTS_L(R)_2_1	121	122	rpSTS, rostromedian superior temporal sulcus	-54, - 40, 4	53, - 37, 3	
		pSTS_L(R)_2_2	123	124	cpSTS, caudoposterior superior temporal sulcus	-52, - 50, - 11	57, - 40, 12	
	Parietal Lobe	SPL, Superior Parietal Lobule	SPL_L(R)_5_1	125	126	A7r, rostral area 7	-16, - 60, - 63	19, - 57, 65
			SPL_L(R)_5_2	127	128	A7c, caudal area 7	-15, - 71, - 52	19, - 69, 54
			SPL_L(R)_5_3	129	130	A5l, lateral area 5	-33, - 47, - 50	35, - 42, 54
SPL_L(R)_5_4			131	132	A7pc, postcentral area 7	-22, - 47, - 65	23, - 43, 67	

		SPL_L(R)_5_5	133	134	A7ip, intraparietal area 7(hIP3)	-27, -59, 54	31, -54, 53
	IPL, Inferior Parietal Lobule	IPL_L(R)_6_1	135	136	A39c, caudal area 39(PGp)	-34, -80, 29	45, -71, 20
		IPL_L(R)_6_2	137	138	A39rd, rostrorodorsal area 39(Hip3)	-38, -61, 46	39, -65, 44
		IPL_L(R)_6_3	139	140	A40rd, rostrorodorsal area 40(PFt)	-51, -33, 42	47, -35, 45
		IPL_L(R)_6_4	141	142	A40c, caudal area 40(PFm)	-56, -49, 38	57, -44, 38
		IPL_L(R)_6_5	143	144	A39rv, rostroventral area 39(PGa)	-47, -65, 26	53, -54, 25
		IPL_L(R)_6_6	145	146	A40rv, rostroventral area 40(PFop)	-53, -31, 23	55, -26, 26
	Pcun, Precuneus	PCun_L(R)_4_1	147	148	A7m, medial area 7(PEp)	-5, -63, 51	6, -65, 51
		PCun_L(R)_4_2	149	150	A5m, medial area 5(PEm)	-8, -47, 57	7, -47, 58
		PCun_L(R)_4_3	151	152	dmPOS, dorsomedial parietooccipital sulcus(P Er)	-12, -67, 25	16, -64, 25
		PCun_L(R)_4_4	153	154	A31, area 31 (Lc1)	-6, -55, 34	6, -54, 35
	PoG, Postcentral Gyrus	PoG_L(R)_4_1	155	156	A1/2/3ulhf, area 1/2/3(upper limb, head and face region)	-50, -16, 43	50, -14, 44
		PoG_L(R)_4_2	157	158	A1/2/3tonla, area 1/2/3(tongue and larynx region)	-56, -14, 16	56, -10, 15
		PoG_L(R)_4_3	159	160	A2, area 2	-46, -30, 50	48, -24, 48
		PoG_L(R)_4_4	161	162	A1/2/3tru, area 1/2/3(trunk region)	-21, -35, 68	20, -33, 69
Insular Lobe	INS, Insular Gyrus	INS_L(R)_6_1	163	164	G, hypergranular insula	-36, -20, 10	37, -18, 8
		INS_L(R)_6_2	165	166	vIa, ventral agranular insula	-32, 14, -13	33, 14, -13
		INS_L(R)_6_3	167	168	dIa, dorsal agranular insula	-34, 18, 1	36, 18, 1
		INS_L(R)_6_4	169	170	vId/vIg, ventral dysgranular and granular insula	-38, -4, -9	39, -2, -9
		INS_L(R)_6_5	171	172	dIg, dorsal granular insula	-38, -8, 8	39, -7, 8
		INS_L(R)_6_6	173	174	dId, dorsal dysgranular insula	-38, 5, 5	38, 5, 5

Limbic Lobe	CG, Cingulate Gyrus	CG_L(R)_7_1	175	176	A23d, dorsal area 23	-4, -39, 31	-	4, -37, 32
		CG_L(R)_7_2	177	178	A24rv, rostroventral area 24	-3, 25	8,	5, 22, 12
		CG_L(R)_7_3	179	180	A32p, pregenual area 32	-6, 34, 21		5, 28, 27
		CG_L(R)_7_4	181	182	A23v, ventral area 23	-8, 47, 10	-	9, -44, 11
		CG_L(R)_7_5	183	184	A24cd, caudodorsal area 24	-5, 37	7,	4, 6, 38
		CG_L(R)_7_6	185	186	A23c, caudal area 23	-7, 23, 41	-	6, -20, 40
		CG_L(R)_7_7	187	188	A32sg, subgenual area 32	-4, 39, -2		5, 41, 6
Occipital Lobe	MVOcC, MedioVentral Occipital Cortex	MVOcC_L(R)_5_1	189	190	cLinG, caudal lingual gyrus	-11, 82, 11	-	10, -85, -9
		MVOcC_L(R)_5_2	191	192	rCunG, rostral cuneus gyrus	-5, 81, 10	-	7, -76, 11
		MVOcC_L(R)_5_3	193	194	cCunG, caudal cuneus gyrus	-6, 94, 1	-	8, -90, 12
		MVOcC_L(R)_5_4	195	196	rLinG, rostral lingual gyrus	-17, 60, -6	-	18, -60, -7
		MVOcC_L(R)_5_5	197	198	vmPOS, ventromedial parietooccipital sulcus	-13, 68, 12	-	15, -63, 12
	LOcC, lateral Occipital Cortex	LOcC_L(R)_4_1	199	200	mOccG, middle occipital gyrus	-31, 89, 11	-	34, -86, 11
		LOcC_L(R)_4_2	201	202	V5/MT+, area V5/MT+	-46, 74, 3	-	48, -70, -1
		LOcC_L(R)_4_3	203	204	OPC, occipital polar cortex	-18, 99, 2	-	22, -97, 4
		LOcC_L(R)_4_4	205	206	iOccG, inferior occipital gyrus	-30, 88, 12	-	32, -85, -12
		LOcC_L(R)_2_1	207	208	msOccG, medial superior occipital gyrus	-11, 88, 31	-	16, -85, 34
		LOcC_L(R)_2_2	209	210	lsOccG, lateral superior occipital gyrus	-22, 77, 36	-	29, -75, 36
	Subcortical Nuclei	Amyg, Amygdala	Amyg_L(R)_2_1	211	212	mAmyg, medial amygdala	-19, 2, -20	-
Amyg_L(R)_2_2			213	214	lAmyg, lateral amygdala	-27, 4, -20	-	28, -3, -20
Hipp, Hippocampus		Hipp_L(R)_2_1	215	216	rHipp, rostral hippocampus	-22, 14, 19	-	22, -12, -20
		Hipp_L(R)_2_2	217	218	cHipp, caudal hippocampus	-28, 30, 10	-	29, -27, -10
BG, Basal Ganglia		BG_L(R)_6_1	219	220	vCa, ventral caudate	-12, 14, 0		15, 14, -2
		BG_L(R)_6_2	221	222	GP, globus pallidus	-22, 2, 4	-	22, -2, 3

		BG_L(R)_6_3	223	224	NAC, nucleus accumbens	-17, 3, -9	15, 8, -9
		BG_L(R)_6_4	225	226	vmPu, ventromedial putamen	-23, 7, -4	22, 8, -1
		BG_L(R)_6_5	227	228	dCa, dorsal caudate	-14, 2, 16	14, 5, 14
		BG_L(R)_6_6	229	230	dIPu, dorsolateral putamen	-28, -5, 2	29, -3, 1
	Tha, Thalamus	Tha_L(R)_8_1	231	232	mPFtha, medial pre-frontal thalamus	-7, -12, 5	7, -11, 6
		Tha_L(R)_8_2	233	234	mPMtha, pre-motor thalamus	-18, -13, 3	12, -14, 1
		Tha_L(R)_8_3	235	236	Stha, sensory thalamus	-18, -23, 4	18, -22, 3
		Tha_L(R)_8_4	237	238	rTtha, rostral temporal thalamus	-7, -14, 7	3, -13, 5
		Tha_L(R)_8_5	239	240	PPtha, posterior parietal thalamus	-16, -24, 6	15, -25, 6
		Tha_L(R)_8_6	241	242	Otha, occipital thalamus	-15, -28, 4	13, -27, 8
		Tha_L(R)_8_7	243	244	cTtha, caudal temporal thalamus	-12, -22, 13	10, -14, 14
		Tha_L(R)_8_8	245	246	lPFtha, lateral pre-frontal thalamus	-11, -14, 2	13, -16, 7

## Appendix B Regions of Interest with a Significant Difference in Degree Centrality between Older Adults and Younger Adults

<i>ROI</i>	<i>beta</i>	<i>T</i>	<i>dof</i>	<i>p-unc</i>	<i>p-FDR</i>
<i>network</i>	0.0	nan	150	nan	nan
<i>SPL_L_5_4</i>	13.74	7.88	150	0.0	0.0
<i>SPL_R_5_1</i>	11.58	6.25	150	0.0	0.0
<i>PrG_R_6_4</i>	12.78	6.01	150	0.0	1e-06
<i>PCL_R_2_2</i>	12.22	5.76	150	0.0	2e-06
<i>PCL_L_2_2</i>	12.25	5.75	150	0.0	2e-06
<i>PCL_L_2_1</i>	11.65	5.44	150	0.0	9e-06
<i>Tha_R_8_3</i>	-13.39	-5.35	150	0.0	1e-05
<i>PoG_L_4_4</i>	10.18	5.34	150	0.0	1e-05
<i>IPL_R_6_4</i>	8.66	5.04	150	1e-06	3.6e-05
<i>PrG_L_6_3</i>	10.3	4.83	150	3e-06	8.1e-05
<i>PrG_L_6_4</i>	11.01	4.79	150	4e-06	8.9e-05
<i>PoG_R_4_4</i>	9.03	4.72	150	5e-06	0.00011
<i>PhG_R_6_3</i>	-9.6	-4.62	150	8e-06	0.000154
<i>MFG_R_7_5</i>	7.25	4.38	150	2.2e-05	0.000385
<i>PrG_R_6_3</i>	9.87	4.36	150	2.4e-05	0.000385
<i>PhG_L_6_3</i>	-9.09	-4.35	150	2.5e-05	0.000385
<i>SPL_R_5_4</i>	7.68	4.31	150	2.9e-05	0.000418
<i>Tha_L_8_3</i>	-10.1	-4.23	150	4e-05	0.000541
<i>PCun_L_4_2</i>	8.95	4.22	150	4.2e-05	0.000541
<i>MFG_R_7_3</i>	8.32	4.2	150	4.6e-05	0.00057
<i>MFG_L_7_3</i>	7.69	4.13	150	6e-05	0.000699
<i>MFG_R_7_1</i>	7.97	4.03	150	8.9e-05	0.000984
<i>INS_R_6_1</i>	-8.11	-4.02	150	9.2e-05	0.000984
<i>ITG_L_7_1</i>	-10.26	-3.88	150	0.000158	0.001619
<i>Tha_R_8_2</i>	-8.63	-3.77	150	0.000233	0.002171
<i>Tha_R_8_4</i>	-9.4	-3.77	150	0.000235	0.002171
<i>PCL_R_2_1</i>	7.41	3.77	150	0.000238	0.002171
<i>PhG_L_6_1</i>	-10.12	-3.64	150	0.000369	0.003239
<i>PhG_L_6_6</i>	-7.13	-3.63	150	0.000382	0.003239
<i>PhG_R_6_6</i>	-6.9	-3.61	150	0.000413	0.003386
<i>SPL_R_5_5</i>	6.25	3.6	150	0.000434	0.003442
<i>MFG_L_7_1</i>	7.22	3.59	150	0.000449	0.003451
<i>FuG_L_3_1</i>	-8.38	-3.5	150	0.000612	0.004562
<i>MFG_R_7_4</i>	6.67	3.48	150	0.000663	0.004795
<i>Tha_L_8_8</i>	-8.01	-3.39	150	0.000891	0.006266
<i>SPL_L_5_1</i>	6.51	3.38	150	0.000932	0.006372
<i>PCun_R_4_2</i>	7.39	3.37	150	0.00097	0.006449
<i>INS_L_6_4</i>	-8.44	-3.34	150	0.001062	0.006872
<i>BG_R_6_3</i>	-7.11	-3.32	150	0.001117	0.007046
<i>SFG_R_7_4</i>	7.24	3.3	150	0.0012	0.007378
<i>PoG_R_4_1</i>	7.87	3.29	150	0.001251	0.007504
<i>INS_R_6_2</i>	-8.42	-3.27	150	0.001316	0.007706
<i>STG_L_6_1</i>	-7.6	-3.22	150	0.001566	0.008959
<i>PhG_R_6_2</i>	-7.32	-3.09	150	0.002392	0.013372
<i>SFG_R_7_1</i>	6.38	3.07	150	0.002551	0.013947
<i>IFG_R_6_5</i>	6.2	3.06	150	0.002612	0.013969
<i>Tha_L_8_5</i>	-7.03	-3.01	150	0.003067	0.016052
<i>ITG_L_7_7</i>	-6.86	-3.0	150	0.003208	0.016439
<i>PrG_L_6_2</i>	6.56	2.97	150	0.003472	0.017208
<i>Amyg_L_2_1</i>	-8.53	-2.97	150	0.003499	0.017208
<i>SPL_R_5_3</i>	6.42	2.96	150	0.003568	0.017208
<i>MFG_L_7_7</i>	5.15	2.94	150	0.003754	0.017758
<i>SFG_R_7_6</i>	5.34	2.93	150	0.003886	0.017815
<i>Amyg_R_2_1</i>	-7.78	-2.93	150	0.003911	0.017815

<i>CG_R_7_6</i>	5.13	2.88	150	0.00457	0.020439
<i>Tha_R_8_8</i>	-6.04	-2.84	150	0.005212	0.022882
<i>PoG_L_4_1</i>	6.65	2.83	150	0.005302	0.022882
<i>MFG_L_7_5</i>	4.47	2.82	150	0.005521	0.023415
<i>IPL_L_6_2</i>	4.87	2.79	150	0.006023	0.025112
<i>PhG_L_6_2</i>	-6.91	-2.76	150	0.006482	0.026577
<i>CG_R_7_1</i>	4.55	2.73	150	0.007144	0.028202
<i>Tha_L_8_2</i>	-6.17	-2.72	150	0.007399	0.028202
<i>IFG_L_6_2</i>	-5.8	-2.71	150	0.007502	0.028202
<i>INS_L_6_2</i>	-6.55	-2.71	150	0.00754	0.028202
<i>BG_L_6_2</i>	-6.38	-2.71	150	0.007549	0.028202
<i>SPL_L_5_5</i>	5.0	2.71	150	0.007566	0.028202
<i>SPL_R_5_2</i>	4.15	2.69	150	0.007857	0.028849
<i>MTG_R_4_2</i>	-4.97	-2.64	150	0.00911	0.032957
<i>BG_L_6_3</i>	-5.74	-2.62	150	0.009566	0.034105
<i>INS_L_6_1</i>	-4.78	-2.62	150	0.009739	0.034227
<i>PrG_L_6_1</i>	6.23	2.59	150	0.010459	0.03624
<i>MFG_R_7_7</i>	4.39	2.52	150	0.01264	0.042651
<i>LOcC_R_4_2</i>	5.21	2.52	150	0.012657	0.042651
<i>IFG_L_6_1</i>	-5.45	-2.49	150	0.013751	0.045713
<i>SPL_L_5_3</i>	4.53	2.46	150	0.015098	0.049523

*Note.* ROIs = Regions of Interest from the Brainnetome Atlas. The table shows the results of second-level group comparison (Group 3 > Group 1) for the degree centrality. *Beta* indicates the effect size (difference in DC between groups); *T* is the T-statistic from the general linear model; *dof*= degrees of freedom; *p-unc* = uncorrected *p*-value; *p*-values are two-tailed; *p-FDR* = *p*-value corrected for multiple comparisons using the false discovery rate (FDR).

## Appendix C Regions of Interest with a Significant Difference in Degree Centrality between Older Adults and Early Middle- Aged Adults

<i>ROI</i>	<i>beta</i>	<i>T</i>	<i>dof</i>	<i>p-unc</i>	<i>p-FDR</i>
<i>network</i>	-0.0	nan	145	nan	nan
<i>SPL_L_5_4</i>	13.54	6.83	145	0.0	0.0
<i>PoG_L_4_4</i>	10.03	5.05	145	1e-06	0.000157
<i>SPL_R_5_1</i>	9.35	4.68	145	7e-06	0.000414
<i>IPL_L_6_2</i>	7.91	4.67	145	7e-06	0.000414
<i>INS_L_6_2</i>	-11.95	-4.55	145	1.1e-05	0.000511
<i>MFG_R_7_5</i>	7.32	4.53	145	1.2e-05	0.000511
<i>Amyg_R_2_1</i>	-11.03	-4.39	145	2.2e-05	0.000697
<i>Amyg_L_2_1</i>	-12.39	-4.37	145	2.4e-05	0.000697
<i>SPL_R_5_4</i>	8.53	4.35	145	2.6e-05	0.000697
<i>Tha_R_8_3</i>	-10.78	-4.3	145	3.1e-05	0.00076
<i>Tha_R_8_4</i>	-11.17	-4.22	145	4.3e-05	0.000969
<i>INS_R_6_1</i>	-8.38	-3.95	145	0.000121	0.002478
<i>Tha_R_8_2</i>	-9.63	-3.92	145	0.000137	0.002599
<i>PoG_R_4_4</i>	8.2	3.83	145	0.000192	0.003377
<i>MFG_L_7_3</i>	7.4	3.75	145	0.000257	0.003671
<i>PhG_R_6_3</i>	-7.14	-3.74	145	0.00026	0.003671
<i>SPL_R_5_5</i>	6.61	3.74	145	0.000261	0.003671
<i>MFG_L_7_7</i>	7.12	3.72	145	0.000282	0.003671
<i>INS_R_6_2</i>	-10.54	-3.72	145	0.000284	0.003671
<i>Tha_L_8_5</i>	-9.28	-3.63	145	0.000389	0.004779
<i>CG_R_7_2</i>	-8.16	-3.58	145	0.000476	0.005529
<i>SPL_R_5_3</i>	7.49	3.56	145	0.000495	0.005529
<i>MFG_R_7_1</i>	7.0	3.54	145	0.000547	0.005853
<i>MFG_R_7_4</i>	6.91	3.52	145	0.000585	0.005909
<i>MFG_L_7_1</i>	7.09	3.51	145	0.000601	0.005909
<i>PCL_L_2_1</i>	7.6	3.45	145	0.000734	0.006945
<i>PrG_L_6_3</i>	7.54	3.41	145	0.000856	0.007797
<i>MFG_L_7_5</i>	5.29	3.38	145	0.000933	0.008201
<i>Tha_L_8_8</i>	-8.5	-3.35	145	0.001047	0.008663
<i>Tha_L_8_3</i>	-8.46	-3.34	145	0.001056	0.008663
<i>PrG_R_6_3</i>	7.69	3.31	145	0.001161	0.009215
<i>PrG_R_6_4</i>	7.65	3.28	145	0.001311	0.010075
<i>PhG_L_6_3</i>	-6.39	-3.15	145	0.002011	0.014989
<i>INS_L_6_4</i>	-7.65	-3.04	145	0.002833	0.019665
<i>PCun_L_4_2</i>	6.28	3.03	145	0.002858	0.019665
<i>Hipp_L_2_1</i>	-7.01	-3.03	145	0.002878	0.019665
<i>MVOcC_L_5_3</i>	5.62	2.89	145	0.004434	0.029482
<i>PCL_R_2_2</i>	6.5	2.87	145	0.004714	0.030138
<i>PCun_R_4_2</i>	6.13	2.86	145	0.00481	0.030138
<i>IPL_R_6_4</i>	5.23	2.86	145	0.0049	0.030138
<i>STG_R_6_5</i>	-6.47	-2.83	145	0.005295	0.031767
<i>PrG_L_6_4</i>	6.56	2.82	145	0.005524	0.031937
<i>MFG_R_7_3</i>	6.15	2.81	145	0.005583	0.031937
<i>INS_L_6_1</i>	-5.3	-2.8	145	0.005762	0.031937
<i>IFG_R_6_5</i>	5.82	2.8	145	0.005842	0.031937
<i>OrG_L_6_5</i>	-8.69	-2.78	145	0.006106	0.032656
<i>SFG_R_7_4</i>	5.95	2.77	145	0.006356	0.033265
<i>MFG_L_7_4</i>	4.62	2.7	145	0.007697	0.039449
<i>PrG_L_6_2</i>	6.19	2.66	145	0.008805	0.044203
<i>BG_L_6_2</i>	-5.82	-2.64	145	0.009194	0.045236
<i>CG_R_7_1</i>	4.42	2.62	145	0.009663	0.046045
<i>MTG_R_4_4</i>	-5.13	-2.61	145	0.009877	0.046045

<i>CG_R_7_3</i>	4.81	2.61	145	0.00992	0.046045
<i>PhG_L_6_1</i>	-7.21	-2.58	145	0.010935	0.049816

*Note.* ROIs = Regions of Interest from the Brainnetome Atlas. The table shows the results of second-level group comparison (Group 3 > Group 2) for the degree centrality. *Beta* indicates the effect size (difference in DC between groups); *T* is the T-statistic from the general linear model; *dof*= degrees of freedom; *p-unc* = uncorrected *p*-value; *p*-values are two-tailed; *p-FDR* = *p*-value corrected for multiple comparisons using the false discovery rate (FDR).

## Appendix D Regions of Interest with a Significant Difference in Global Efficiency between Older Adults and Younger Adults

<i>ROI</i>	<i>beta</i>	<i>T</i>	<i>dof</i>	<i>p-unc</i>	<i>p-FDR</i>
<i>network</i>	-0.01	-2.69	150	0.007949	nan
<i>PhG_R_6_6</i>	-0.03	-5.74	150	0.0	1.2e-05
<i>SPL_L_5_4</i>	0.02	5.54	150	0.0	1.6e-05
<i>PCL_R_2_2</i>	0.03	5.35	150	0.0	2.6e-05
<i>PhG_L_6_3</i>	-0.03	-5.13	150	1e-06	5.1e-05
<i>PCL_L_2_2</i>	0.02	5.09	150	1e-06	5.1e-05
<i>PrG_R_6_4</i>	0.02	5.05	150	1e-06	5.2e-05
<i>Tha_R_8_4</i>	-0.03	-5.01	150	2e-06	5.4e-05
<i>Tha_R_8_3</i>	-0.05	-4.92	150	2e-06	6.8e-05
<i>INS_R_6_1</i>	-0.03	-4.73	150	5e-06	0.000131
<i>PhG_R_6_3</i>	-0.03	-4.72	150	5e-06	0.000131
<i>SPL_R_5_1</i>	0.02	4.64	150	7e-06	0.000167
<i>PhG_L_6_1</i>	-0.04	-4.5	150	1.4e-05	0.000281
<i>FuG_L_3_1</i>	-0.03	-4.47	150	1.6e-05	0.000288
<i>PrG_L_6_4</i>	0.02	4.45	150	1.6e-05	0.000288
<i>PhG_L_6_6</i>	-0.03	-4.39	150	2.1e-05	0.000342
<i>ITG_L_7_1</i>	-0.05	-4.36	150	2.4e-05	0.00035
<i>Tha_R_8_2</i>	-0.03	-4.36	150	2.4e-05	0.00035
<i>STG_R_6_3</i>	-0.02	-4.34	150	2.6e-05	0.000362
<i>PrG_L_6_3</i>	0.02	4.25	150	3.8e-05	0.000469
<i>Amyg_L_2_1</i>	-0.03	-4.25	150	3.8e-05	0.000469
<i>PoG_L_4_4</i>	0.02	4.19	150	4.8e-05	0.000546
<i>INS_L_6_4</i>	-0.03	-4.18	150	4.9e-05	0.000546
<i>PoG_R_4_4</i>	0.02	4.13	150	5.9e-05	0.000632
<i>INS_L_6_5</i>	-0.02	-4.1	150	6.8e-05	0.000696
<i>INS_L_6_1</i>	-0.02	-4.08	150	7.2e-05	0.000706
<i>PCL_L_2_1</i>	0.02	4.02	150	9.3e-05	0.000879
<i>Tha_L_8_3</i>	-0.06	-3.9	150	0.000143	0.001303
<i>INS_R_6_2</i>	-0.04	-3.84	150	0.000179	0.001576
<i>STG_L_6_3</i>	-0.02	-3.77	150	0.000236	0.002005
<i>STG_L_6_1</i>	-0.02	-3.61	150	0.00042	0.003442
<i>Amyg_R_2_1</i>	-0.03	-3.56	150	0.000497	0.00386
<i>FuG_R_3_1</i>	-0.02	-3.55	150	0.000513	0.00386
<i>Tha_R_8_5</i>	-0.02	-3.55	150	0.000518	0.00386
<i>STG_R_6_2</i>	-0.02	-3.52	150	0.000567	0.003925
<i>Tha_R_8_8</i>	-0.02	-3.52	150	0.000571	0.003925
<i>Tha_L_8_8</i>	-0.03	-3.52	150	0.000574	0.003925
<i>PrG_R_6_3</i>	0.02	3.48	150	0.000659	0.004359
<i>Tha_L_8_5</i>	-0.03	-3.47	150	0.000673	0.004359
<i>Tha_L_8_6</i>	-0.02	-3.45	150	0.000738	0.00457
<i>ITG_L_7_7</i>	-0.04	-3.44	150	0.000743	0.00457
<i>MFG_R_7_1</i>	0.02	3.38	150	0.000928	0.005448
<i>PhG_R_6_2</i>	-0.04	-3.38	150	0.00093	0.005448
<i>MFG_R_7_3</i>	0.02	3.3	150	0.001218	0.006967
<i>BG_R_6_3</i>	-0.02	-3.29	150	0.001254	0.006984
<i>INS_R_6_5</i>	-0.02	-3.28	150	0.001277	0.006984
<i>Hipp_R_2_1</i>	-0.02	-3.18	150	0.001818	0.009722
<i>STG_L_6_5</i>	-0.02	-3.15	150	0.001966	0.010289
<i>BG_R_6_2</i>	-0.02	-3.13	150	0.002126	0.010894
<i>MTG_R_4_2</i>	-0.01	-3.11	150	0.002252	0.011307
<i>IFG_L_6_1</i>	-0.02	-3.08	150	0.002454	0.011756
<i>IPL_R_6_4</i>	0.01	3.08	150	0.002466	0.011756
<i>Tha_L_8_2</i>	-0.03	-3.08	150	0.002485	0.011756
<i>INS_R_6_6</i>	-0.02	-3.03	150	0.002851	0.013231
<i>IFG_L_6_2</i>	-0.02	-3.01	150	0.003038	0.013841
<i>Hipp_L_2_1</i>	-0.02	-2.97	150	0.003456	0.015457

<i>INS_R_6_4</i>	-0.02	-2.96	150	0.003595	0.015794
<i>FuG_R_3_2</i>	-0.01	-2.94	150	0.003745	0.016164
<i>OrG_L_6_5</i>	-0.03	-2.9	150	0.004284	0.01817
<i>OrG_L_6_3</i>	-0.02	-2.89	150	0.004401	0.018349
<i>PhG_L_6_2</i>	-0.04	-2.88	150	0.004509	0.018489
<i>BG_L_6_3</i>	-0.02	-2.87	150	0.00469	0.018914
<i>PoG_R_4_1</i>	0.01	2.86	150	0.004844	0.019143
<i>IPL_L_6_5</i>	-0.01	-2.86	150	0.004903	0.019143
<i>BG_L_6_2</i>	-0.02	-2.84	150	0.005095	0.019582
<i>INS_L_6_2</i>	-0.03	-2.8	150	0.005707	0.021598
<i>MFG_L_7_3</i>	0.01	2.76	150	0.006518	0.024262
<i>FuG_R_3_3</i>	-0.01	-2.75	150	0.006608	0.024262
<i>PhG_L_6_4</i>	-0.04	-2.69	150	0.007868	0.028463
<i>ITG_R_7_1</i>	-0.02	-2.64	150	0.009113	0.032489
<i>MFG_R_7_5</i>	0.01	2.63	150	0.00934	0.032823
<i>MFG_L_7_1</i>	0.01	2.62	150	0.009808	0.033984
<i>IPL_L_6_3</i>	-0.01	-2.56	150	0.011385	0.038597
<i>Amyg_L_2_2</i>	-0.02	-2.56	150	0.011453	0.038597
<i>PCun_L_4_2</i>	0.01	2.55	150	0.011852	0.0394
<i>BG_L_6_4</i>	-0.02	-2.54	150	0.012099	0.039684
<i>SFG_R_7_4</i>	0.01	2.53	150	0.012568	0.04068
<i>BG_L_6_1</i>	-0.02	-2.51	150	0.01307	0.041756
<i>MTG_L_4_3</i>	-0.01	-2.51	150	0.01325	0.041789
<i>MVOcC_R_5_4</i>	-0.02	-2.5	150	0.013625	0.041924
<i>CG_R_7_2</i>	-0.02	-2.5	150	0.013634	0.041924
<i>STG_R_6_5</i>	-0.01	-2.48	150	0.014382	0.043665
<i>PhG_R_6_1</i>	-0.03	-2.47	150	0.014729	0.043665
<i>OrG_R_6_3</i>	-0.01	-2.47	150	0.014732	0.043665
<i>CG_L_7_4</i>	-0.01	-2.45	150	0.015604	0.045699
<i>pSTS_R_2_2</i>	-0.01	-2.43	150	0.016308	0.047196
<i>PoG_L_4_1</i>	0.01	2.41	150	0.017019	0.048681
<i>OrG_L_6_2</i>	-0.01	-2.41	150	0.017319	0.048846
<i>SPL_R_5_4</i>	0.01	2.4	150	0.017571	0.048846
<i>PCun_R_4_2</i>	0.01	2.4	150	0.017672	0.048846

Note. ROIs = Regions of Interest from the Brainnetome Atlas. The table shows the results of second-level group comparison (Group 3 > Group 1) for the global efficiency (GE). *Beta* indicates the effect size (difference in GE between groups); *T* is the T-statistic from the general linear model; *dof*= degrees of freedom; *p-unc* = uncorrected *p*-value; *p*-values are two-tailed; *p-FDR* = *p*-value corrected for multiple comparisons using the false discovery rate (FDR).

## Appendix E Regions of Interest with a Significant Difference in Global Efficiency between Older Adults and Early Middle- Aged Adults

<i>ROI</i>	<i>beta</i>	<i>T</i>	<i>dof</i>	<i>p-unc</i>	<i>p-FDR</i>
<i>network</i>	-0.0	-1.85	145	0.065675	nan
<i>Amyg_L_2_1</i>	-0.04	-5.39	145	0.0	5.8e-05
<i>Amyg_R_2_1</i>	-0.03	-5.27	145	0.0	5.8e-05
<i>SPL_L_5_4</i>	0.03	5.19	145	1e-06	5.8e-05
<i>Tha_R_8_4</i>	-0.03	-5.07	145	1e-06	7.3e-05
<i>PoG_L_4_4</i>	0.02	4.51	145	1.3e-05	0.00066
<i>INS_R_6_1</i>	-0.03	-4.45	145	1.7e-05	0.000696
<i>Tha_R_8_2</i>	-0.03	-4.12	145	6.3e-05	0.001935
<i>PhG_R_6_3</i>	-0.03	-4.12	145	6.3e-05	0.001935
<i>SPL_R_5_1</i>	0.02	4.07	145	7.8e-05	0.002133
<i>INS_L_6_1</i>	-0.02	-3.92	145	0.000139	0.003184
<i>PhG_L_6_3</i>	-0.02	-3.91	145	0.000142	0.003184
<i>Tha_L_8_5</i>	-0.03	-3.87	145	0.000165	0.003379
<i>Hipp_L_2_1</i>	-0.02	-3.77	145	0.000233	0.004406
<i>MVOcC_L_5_3</i>	0.02	3.73	145	0.000279	0.004903
<i>INS_R_6_2</i>	-0.04	-3.63	145	0.000393	0.00644
<i>INS_L_6_2</i>	-0.04	-3.59	145	0.000455	0.006957
<i>STG_R_6_5</i>	-0.02	-3.57	145	0.000481	0.006957
<i>PoG_R_4_4</i>	0.02	3.53	145	0.000559	0.007646
<i>INS_L_6_5</i>	-0.02	-3.47	145	0.000695	0.009001
<i>Tha_L_8_3</i>	-0.06	-3.42	145	0.000807	0.009931
<i>INS_L_6_4</i>	-0.03	-3.38	145	0.000934	0.010942
<i>Tha_L_8_8</i>	-0.03	-3.28	145	0.001321	0.014768
<i>PhG_R_6_6</i>	-0.02	-3.21	145	0.001613	0.017022
<i>MFG_R_7_5</i>	0.01	3.21	145	0.001661	0.017022
<i>MFG_L_7_3</i>	0.02	3.18	145	0.001773	0.017446
<i>IPL_L_6_2</i>	0.01	3.17	145	0.001851	0.017514
<i>CG_R_7_2</i>	-0.03	-3.14	145	0.002021	0.01841
<i>MFG_R_7_1</i>	0.02	3.12	145	0.002214	0.019449
<i>IPL_L_6_6</i>	-0.01	-3.04	145	0.002789	0.023656
<i>MFG_L_7_1</i>	0.02	3.02	145	0.003029	0.024841
<i>SPL_R_5_4</i>	0.01	2.98	145	0.003381	0.025635
<i>ITG_L_7_1</i>	-0.03	-2.96	145	0.0036	0.025635
<i>MTG_R_4_4</i>	-0.01	-2.96	145	0.003619	0.025635
<i>BG_L_6_2</i>	-0.02	-2.95	145	0.003708	0.025635
<i>OrG_L_6_5</i>	-0.04	-2.95	145	0.003734	0.025635
<i>Hipp_R_2_1</i>	-0.02	-2.95	145	0.003751	0.025635
<i>STG_R_6_6</i>	-0.01	-2.93	145	0.003991	0.026146
<i>PCL_L_2_1</i>	0.02	2.92	145	0.004039	0.026146
<i>PrG_R_6_3</i>	0.02	2.84	145	0.005158	0.032534
<i>PrG_L_6_3</i>	0.01	2.81	145	0.005651	0.034561
<i>Hipp_R_2_2</i>	-0.02	-2.8	145	0.00576	0.034561
<i>INS_R_6_5</i>	-0.02	-2.78	145	0.006123	0.035862
<i>OrG_L_6_2</i>	-0.02	-2.77	145	0.00632	0.036156
<i>Tha_R_8_3</i>	-0.04	-2.73	145	0.007077	0.039566
<i>INS_R_6_4</i>	-0.02	-2.71	145	0.007573	0.041398
<i>STG_R_6_4</i>	-0.01	-2.68	145	0.008202	0.043863
<i>FuG_L_3_1</i>	-0.02	-2.65	145	0.008922	0.045538
<i>MTG_R_4_2</i>	-0.01	-2.65	145	0.009042	0.045538
<i>Tha_R_8_8</i>	-0.02	-2.64	145	0.009071	0.045538
<i>PhG_L_6_6</i>	-0.02	-2.63	145	0.009491	0.046694
<i>SPL_R_5_5</i>	0.01	2.6	145	0.010317	0.047293
<i>SPL_R_5_3</i>	0.01	2.6	145	0.010325	0.047293
<i>Tha_R_8_5</i>	-0.02	-2.6	145	0.010388	0.047293

<i>MFG_R_7_3</i>	0.01	2.6	145	0.010408	0.047293
<i>PrG_L_6_2</i>	0.01	2.58	145	0.010753	0.047293
<i>MFG_L_7_7</i>	0.01	2.58	145	0.010887	0.047293
<i>IFG_L_6_1</i>	-0.01	-2.58	145	0.010958	0.047293
<i>PhG_L_6_4</i>	-0.04	-2.57	145	0.01124	0.047406
<i>PCL_R_2_2</i>	0.01	2.56	145	0.01137	0.047406
<i>PrG_R_6_4</i>	0.01	2.54	145	0.012055	0.049424

*Note.* ROIs = Regions of Interest from the Brainnetome Atlas. The table shows the results of second-level group comparison (Group 3 > Group 2) for the global efficiency (GE). *Beta* indicates the effect size (difference in GE between groups); *T* is the T-statistic from the general linear model; *dof* = degrees of freedom; *p-unc* = uncorrected *p*-value; *p*-values are two-tailed; *p-FDR* = *p*-value corrected for multiple comparisons using the false discovery rate (FDR).

## Appendix F    Regions of Interest with a Significant Difference in Local Efficiency between Older Adults and Younger Adults

<i>ROI</i>	<i>beta</i>	<i>T</i>	<i>dof</i>	<i>p-unc</i>	<i>p-FDR</i>
<i>network</i>	0.01	2.34	150	0.020767	nan
<i>INS_L_6_4</i>	0.04	5.64	150	0.0	1.3e-05
<i>SPL_L_5_4</i>	0.04	5.59	150	0.0	1.3e-05
<i>SPL_R_5_4</i>	0.04	5.05	150	1e-06	0.000106
<i>INS_R_6_4</i>	0.03	4.48	150	1.5e-05	0.000921
<i>FuG_L_3_3</i>	0.03	4.07	150	7.5e-05	0.003707
<i>CG_R_7_6</i>	0.03	3.93	150	0.00013	0.005013
<i>PoG_R_4_3</i>	0.03	3.89	150	0.000151	0.005013
<i>MFG_R_7_1</i>	0.03	3.86	150	0.000171	0.005013
<i>SFG_R_7_4</i>	0.03	3.84	150	0.000183	0.005013
<i>INS_R_6_1</i>	0.03	3.65	149	0.000359	0.008835
<i>PoG_L_4_3</i>	0.03	3.61	150	0.000412	0.009221
<i>ITG_R_7_5</i>	0.02	3.57	150	0.000488	0.009451
<i>STG_R_6_2</i>	0.03	3.54	150	0.000536	0.009451
<i>OrG_L_6_3</i>	0.03	3.54	150	0.000538	0.009451
<i>INS_R_6_3</i>	0.02	3.48	150	0.000665	0.010611
<i>STG_R_6_3</i>	0.03	3.47	150	0.00069	0.010611
<i>PhG_R_6_6</i>	0.03	3.44	150	0.000745	0.010677
<i>INS_L_6_5</i>	0.03	3.42	150	0.000794	0.010677
<i>PCun_L_4_2</i>	0.03	3.41	150	0.000825	0.010677
<i>SPL_R_5_1</i>	0.02	3.39	150	0.000901	0.010921
<i>INS_L_6_1</i>	0.03	3.37	150	0.00094	0.010921
<i>PCL_R_2_1</i>	0.03	3.36	150	0.000977	0.010921
<i>OrG_R_6_3</i>	0.02	3.34	150	0.001075	0.011496
<i>LOcC_R_4_2</i>	0.03	3.29	150	0.00123	0.012609
<i>FuG_R_3_3</i>	0.03	3.22	150	0.001578	0.015531
<i>OrG_L_6_5</i>	0.03	3.19	149	0.001763	0.01668
<i>STG_L_6_3</i>	0.02	3.17	150	0.001876	0.017091
<i>SFG_L_7_6</i>	0.02	3.15	150	0.001948	0.017115
<i>ITG_R_7_2</i>	0.03	3.12	150	0.002161	0.018331
<i>IPL_L_6_5</i>	0.02	3.03	150	0.002838	0.022901
<i>MTG_R_4_1</i>	0.02	3.03	150	0.002909	0.022901
<i>PCun_R_4_2</i>	0.02	3.02	150	0.002979	0.022901
<i>INS_L_6_3</i>	0.02	3.01	150	0.003102	0.023122
<i>IPL_R_6_2</i>	0.02	2.99	150	0.003281	0.023496
<i>CG_L_7_7</i>	0.02	2.98	150	0.003343	0.023496
<i>MFG_R_7_3</i>	0.02	2.96	150	0.003581	0.024186
<i>CG_R_7_4</i>	0.02	2.95	150	0.003638	0.024186
<i>MFG_L_7_1</i>	0.02	2.94	150	0.003812	0.024679
<i>SPL_R_5_5</i>	0.02	2.93	150	0.003938	0.02484
<i>IPL_R_6_3</i>	0.02	2.79	150	0.005916	0.036385
<i>LOcC_R_2_2</i>	0.02	2.75	150	0.006634	0.039802
<i>LOcC_L_2_1</i>	0.02	2.74	150	0.006936	0.040624
<i>ITG_L_7_6</i>	0.02	2.73	150	0.007113	0.040691
<i>IPL_R_6_4</i>	0.01	2.71	150	0.007484	0.041843
<i>CG_L_7_6</i>	0.02	2.69	150	0.007897	0.043168

*Note.* ROIs = Regions of Interest from the Brainnetome Atlas. The table shows the results of second-level group comparison (Group 3 > Group 1) for the local efficiency (LE). *Beta* indicates the effect size (difference in LE between groups); *T* is the T-statistic from the general linear model; *dof* = degrees of freedom; *p-unc* = uncorrected *p*-value; *p*-values are two-tailed; *p-FDR* = *p*-value corrected for multiple comparisons using the false discovery rate (FDR).

## Appendix G Regions of Interest with a Significant Difference in Local Efficiency between Older Adults and Early Middle-Aged Adults

<i>ROI</i>	<i>beta</i>	<i>T</i>	<i>dof</i>	<i>p-unc</i>	<i>p-FDR</i>
<i>network</i>	0.01	1.66	145	0.098821	nan
<i>SPL_R_5_4</i>	0.04	4.92	145	2e-06	0.000577
<i>INS_L_6_4</i>	0.03	4.16	145	5.4e-05	0.006612
<i>SFG_L_7_6</i>	0.02	3.99	145	0.000104	0.008526
<i>ITG_L_7_6</i>	0.03	3.81	145	0.000208	0.010439
<i>ITG_R_7_5</i>	0.02	3.76	145	0.000245	0.010439
<i>SPL_L_5_4</i>	0.03	3.72	145	0.000279	0.010439
<i>IPL_R_6_2</i>	0.02	3.71	145	0.000297	0.010439
<i>MTG_R_4_3</i>	0.03	3.56	145	0.000499	0.015331
<i>INS_R_6_4</i>	0.03	3.31	145	0.001194	0.03118
<i>INS_R_6_1</i>	0.03	3.29	144	0.001267	0.03118
<i>ITG_R_7_6</i>	0.02	3.24	145	0.001485	0.033202
<i>CG_R_7_4</i>	0.02	3.13	145	0.002118	0.041446
<i>PoG_R_4_3</i>	0.03	3.12	145	0.00219	0.041446
<i>MTG_R_4_1</i>	0.02	3.06	145	0.002605	0.045775

*Note.* ROIs = Regions of Interest from the Brainnetome Atlas. The table shows the results of second-level group comparison (Group 3 > Group 2) for the local efficiency (LE). *Beta* indicates the effect size (difference in LE between groups); *T* is the T-statistic from the general linear model; *dof* = degrees of freedom; *p-unc* = uncorrected *p*-value; *p*-values are two-tailed; *p-FDR* = *p*-value corrected for multiple comparisons using the false discovery rate (FDR).

## Appendix H Regions of Interest with a Significant Difference in Clustering Coefficient between Older Adults and Younger Adults

<i>ROI</i>	<i>beta</i>	<i>T</i>	<i>dof</i>	<i>p-unc</i>	<i>p-FDR</i>
<i>network</i>	0.02	2.96	150	0.003545	nan
<i>INS_L_6_4</i>	0.08	6.09	150	0.0	2e-06
<i>SPL_L_5_4</i>	0.08	5.48	150	0.0	2.1e-05
<i>SPL_R_5_4</i>	0.08	5.03	150	1e-06	0.000112
<i>INS_R_6_4</i>	0.06	4.56	150	1.1e-05	0.000663
<i>FuG_L_3_3</i>	0.05	4.36	150	2.4e-05	0.001182
<i>PoG_R_4_3</i>	0.06	4.06	150	7.8e-05	0.003066
<i>OrG_L_6_3</i>	0.05	4.03	150	8.7e-05	0.003066
<i>PhG_R_6_6</i>	0.06	4.0	150	0.0001	0.003066
<i>SFG_R_7_4</i>	0.05	3.93	150	0.000131	0.00354
<i>OrG_R_6_3</i>	0.05	3.9	150	0.000144	0.00354
<i>OrG_L_6_5</i>	0.07	3.88	149	0.000159	0.003555
<i>MFG_R_7_1</i>	0.05	3.81	150	0.000199	0.003817
<i>CG_R_7_6</i>	0.05	3.8	150	0.000213	0.003817
<i>INS_R_6_1</i>	0.06	3.79	149	0.000218	0.003817
<i>INS_R_6_3</i>	0.04	3.77	150	0.000233	0.003817
<i>INS_L_6_1</i>	0.06	3.62	150	0.000404	0.005586
<i>PoG_L_4_3</i>	0.06	3.62	150	0.000406	0.005586
<i>ITG_R_7_5</i>	0.04	3.62	150	0.000409	0.005586
<i>STG_R_6_2</i>	0.06	3.57	150	0.000485	0.006281
<i>INS_L_6_5</i>	0.06	3.55	150	0.000518	0.006314
<i>STG_R_6_3</i>	0.05	3.54	150	0.000539	0.006314
<i>PCun_L_4_2</i>	0.05	3.46	150	0.000699	0.007816
<i>SPL_R_5_1</i>	0.04	3.39	150	0.000884	0.009456
<i>FuG_R_3_3</i>	0.05	3.33	150	0.001083	0.011105
<i>LOcC_R_4_2</i>	0.05	3.31	150	0.001179	0.011597
<i>STG_L_6_3</i>	0.05	3.28	150	0.001298	0.012279
<i>PCL_R_2_1</i>	0.05	3.26	150	0.001398	0.012734
<i>CG_L_7_6</i>	0.05	3.2	150	0.001676	0.014157
<i>IPL_L_6_5</i>	0.04	3.2	150	0.001691	0.014157
<i>CG_L_7_7</i>	0.04	3.19	150	0.001726	0.014157
<i>ITG_L_7_6</i>	0.04	3.12	150	0.002157	0.017108
<i>ITG_R_7_2</i>	0.05	3.1	150	0.002332	0.017108
<i>SFG_L_7_6</i>	0.03	3.1	150	0.002337	0.017108
<i>PCun_R_4_2</i>	0.05	3.09	150	0.00241	0.017108
<i>MTG_R_4_1</i>	0.04	3.08	150	0.002434	0.017108
<i>LOcC_L_2_1</i>	0.05	3.07	150	0.002504	0.017108
<i>INS_L_6_3</i>	0.04	3.05	150	0.002689	0.017877
<i>IPL_R_6_2</i>	0.03	3.04	150	0.002766	0.017906
<i>CG_R_7_4</i>	0.04	3.0	150	0.00314	0.019807
<i>MFG_L_7_1</i>	0.04	2.95	150	0.003633	0.022185
<i>SPL_R_5_5</i>	0.04	2.95	150	0.003697	0.022185
<i>IPL_R_6_3</i>	0.03	2.93	150	0.003953	0.023154
<i>CG_L_7_2</i>	0.04	2.86	149	0.004855	0.027773
<i>CG_R_7_2</i>	0.04	2.81	149	0.005598	0.031299
<i>LOcC_R_2_2</i>	0.04	2.77	150	0.006376	0.034853
<i>MFG_R_7_3</i>	0.03	2.7	150	0.007627	0.040788
<i>SPL_R_5_3</i>	0.04	2.69	150	0.007866	0.04117
<i>PhG_L_6_6</i>	0.04	2.68	150	0.008265	0.04236
<i>Tha_R_8_4</i>	0.05	2.65	150	0.009	0.045186
<i>OrG_L_6_2</i>	0.03	2.63	150	0.009386	0.046179
<i>IPL_R_6_4</i>	0.03	2.62	150	0.009746	0.047008
<i>MFG_L_7_4</i>	0.03	2.6	150	0.010365	0.049034

Note. ROIs = Regions of Interest from the Brainnetome Atlas. The table shows the results of second-level group comparison (Group 3 > Group 1) for the cluster coefficient (CC). *Beta* indicates the effect size (difference in CC between groups); *T* is the T-statistic from the general linear model; *dof*= degrees of freedom; *p-unc* = uncorrected *p*-value; *p*-values are two-tailed; *p-FDR* = *p*-value corrected for multiple comparisons using the false discovery rate (FDR).

## Appendix I Regions of Interest with a Significant Difference in Clustering Coefficient between Older Adults and Early Middle-Aged Adults

<i>ROI</i>	<i>beta</i>	<i>T</i>	<i>dof</i>	<i>p-unc</i>	<i>p-FDR</i>
<i>network</i>	0.02	2.2	145	0.029578	nan
<i>SPL_R_5_4</i>	0.07	4.81	145	4e-06	0.000925
<i>INS_L_6_4</i>	0.07	4.57	145	1e-05	0.001253
<i>ITG_L_7_6</i>	0.05	4.16	145	5.4e-05	0.0044
<i>INS_R_6_4</i>	0.06	4.02	145	9.3e-05	0.004802
<i>SFG_L_7_6</i>	0.04	4.01	145	9.8e-05	0.004802
<i>ITG_R_7_5</i>	0.04	3.81	145	0.000206	0.008203
<i>IPL_R_6_2</i>	0.04	3.77	145	0.000233	0.008203
<i>SPL_L_5_4</i>	0.06	3.65	145	0.000362	0.011135
<i>MTG_R_4_3</i>	0.05	3.54	145	0.000547	0.014957
<i>ITG_R_7_6</i>	0.04	3.5	145	0.000625	0.015383
<i>INS_R_6_1</i>	0.06	3.42	144	0.000805	0.018013
<i>PoG_R_4_3</i>	0.05	3.25	145	0.001425	0.029205
<i>ITG_R_7_2</i>	0.06	3.19	145	0.001754	0.03241
<i>CG_L_7_6</i>	0.05	3.15	145	0.001957	0.03241
<i>SPL_R_5_3</i>	0.05	3.15	145	0.001989	0.03241
<i>CG_R_7_6</i>	0.04	3.11	145	0.002223	0.03241
<i>OrG_R_6_3</i>	0.04	3.11	145	0.00224	0.03241
<i>MTG_R_4_1</i>	0.04	3.09	145	0.002437	0.033224
<i>FuG_R_3_1</i>	0.05	3.06	145	0.002601	0.033224
<i>FuG_L_3_3</i>	0.04	3.05	145	0.002701	0.033224
<i>OrG_L_6_6</i>	0.03	3.01	145	0.003047	0.035695
<i>SPL_R_5_1</i>	0.04	2.96	145	0.003571	0.039931
<i>CG_R_7_4</i>	0.03	2.92	145	0.003999	0.042774
<i>SFG_R_7_6</i>	0.03	2.88	145	0.004527	0.046401
<i>OrG_L_6_2</i>	0.04	2.86	145	0.004864	0.047866

*Note.* ROIs = Regions of Interest from the Brainnetome Atlas. The table shows the results of second-level group comparison (Group 3 > Group 2) for the cluster coefficient (CC). *Beta* indicates the effect size (difference in CC between groups); *T* is the T-statistic from the general linear model; *dof* = degrees of freedom; *p-unc* = uncorrected *p*-value; *p*-values are two-tailed; *p-FDR* = *p*-value corrected for multiple comparisons using the false discovery rate (FDR).

## Appendix J    Regions of Interest with a Significant Difference in Average Path Distance between Older Adults and Younger Adults

<i>ROI</i>	<i>beta</i>	<i>T</i>	<i>dof</i>	<i>p-unc</i>	<i>p-FDR</i>
<i>network</i>	0.03	2.58	150	0.010968	nan
<i>PhG_R_6_6</i>	0.14	6.0	150	0.0	3e-06
<i>PhG_L_6_3</i>	0.11	5.04	150	1e-06	0.000121
<i>STG_R_6_3</i>	0.09	5.02	150	1e-06	0.000121
<i>Tha_R_8_3</i>	0.17	4.81	149	4e-06	0.000229
<i>Tha_R_8_4</i>	0.12	4.7	150	6e-06	0.000266
<i>ITG_L_7_1</i>	0.16	4.68	149	6e-06	0.000266
<i>PhG_L_6_1</i>	0.18	4.59	150	9e-06	0.000303
<i>INS_L_6_4</i>	0.11	4.53	150	1.2e-05	0.000303
<i>FuG_L_3_1</i>	0.1	4.53	150	1.2e-05	0.000303
<i>Amyg_L_2_1</i>	0.11	4.52	150	1.2e-05	0.000303
<i>STG_R_6_2</i>	0.08	4.42	150	1.9e-05	0.000417
<i>STG_L_6_3</i>	0.07	4.4	150	2e-05	0.000417
<i>INS_L_6_1</i>	0.09	4.31	150	3e-05	0.00056
<i>INS_L_6_5</i>	0.09	4.28	150	3.4e-05	0.000582
<i>INS_R_6_1</i>	0.12	4.25	150	3.7e-05	0.000582
<i>PhG_R_6_3</i>	0.12	4.25	150	3.8e-05	0.000582
<i>PhG_L_6_6</i>	0.12	4.19	150	4.8e-05	0.000688
<i>Tha_R_8_2</i>	0.11	4.08	150	7.4e-05	0.001007
<i>OrG_L_6_3</i>	0.08	3.85	150	0.000172	0.002132
<i>FuG_R_3_1</i>	0.1	3.85	150	0.000173	0.002132
<i>Tha_L_8_6</i>	0.11	3.66	150	0.000351	0.00411
<i>INS_R_6_2</i>	0.16	3.58	150	0.000463	0.005179
<i>INS_R_6_4</i>	0.08	3.55	150	0.000515	0.00551
<i>Hipp_R_2_1</i>	0.08	3.53	150	0.000554	0.005675
<i>FuG_L_3_3</i>	0.05	3.46	150	0.00071	0.006982
<i>Tha_R_8_5</i>	0.09	3.45	150	0.00074	0.007001
<i>ITG_L_7_7</i>	0.14	3.39	149	0.000892	0.007851
<i>OrG_L_6_5</i>	0.12	3.39	149	0.000894	0.007851
<i>INS_R_6_5</i>	0.07	3.38	150	0.000932	0.007906
<i>FuG_R_3_2</i>	0.07	3.34	150	0.001072	0.008787
<i>OrG_R_6_3</i>	0.07	3.3	150	0.001222	0.009697
<i>FuG_R_3_3</i>	0.06	3.28	150	0.001308	0.010056
<i>INS_R_6_6</i>	0.06	3.21	150	0.001614	0.012031
<i>PhG_R_6_2</i>	0.13	3.19	148	0.00172	0.012447
<i>STG_L_6_1</i>	0.07	3.15	150	0.001955	0.013421
<i>MTG_L_4_3</i>	0.05	3.15	150	0.001964	0.013421
<i>STG_L_6_5</i>	0.07	3.14	150	0.002062	0.013708
<i>PCL_R_2_2</i>	-0.06	-3.07	150	0.002542	0.016457
<i>ITG_R_7_1</i>	0.12	3.05	150	0.00268	0.01664
<i>Amyg_R_2_1</i>	0.09	3.05	150	0.002706	0.01664
<i>STG_R_6_4</i>	0.05	3.04	150	0.002816	0.016897
<i>Tha_R_8_8</i>	0.07	3.0	150	0.003128	0.018319
<i>Hipp_L_2_1</i>	0.07	2.98	150	0.003372	0.019293
<i>Tha_L_8_5</i>	0.1	2.96	150	0.003586	0.020049
<i>Amyg_L_2_2</i>	0.11	2.95	150	0.003715	0.020306
<i>BG_R_6_2</i>	0.1	2.93	150	0.00389	0.0208
<i>CG_R_7_2</i>	0.07	2.91	149	0.004213	0.021832
<i>Tha_L_8_8</i>	0.1	2.9	150	0.00426	0.021832
<i>Tha_L_8_4</i>	0.06	2.88	150	0.004513	0.022377
<i>pSTS_R_2_2</i>	0.05	2.88	150	0.004548	0.022377
<i>Tha_L_8_2</i>	0.11	2.85	149	0.004921	0.023739
<i>IFG_L_6_1</i>	0.05	2.85	150	0.005025	0.02377
<i>STG_L_6_2</i>	0.05	2.79	150	0.00589	0.026979

<i>MVOcC</i>	0.07	2.79	150	0.005979	0.026979
<i>R_5_4</i>					
<i>IPL_L_6_5</i>	0.05	2.78	150	0.006045	0.026979
<i>Tha_L_8_3</i>	0.13	2.78	145	0.006205	0.026979
<i>IPL_L_6_3</i>	0.04	2.77	150	0.006354	0.026979
<i>INS_R_6_3</i>	0.05	2.77	150	0.006388	0.026979
<i>INS_L_6_2</i>	0.09	2.76	149	0.00647	0.026979
<i>BG_R_6_3</i>	0.09	2.75	150	0.006716	0.027103
<i>CG_L_7_4</i>	0.06	2.75	150	0.006721	0.027103
<i>MTG_R_4_2</i>	0.04	2.74	150	0.006961	0.027621
<i>PrG_L_6_4</i>	-0.05	-2.73	150	0.007095	0.027703
<i>OrG_L_6_2</i>	0.06	2.7	150	0.007706	0.02962
<i>BG_L_6_4</i>	0.07	2.68	150	0.008088	0.030435
<i>STG_R_6_6</i>	0.04	2.68	150	0.008166	0.030435
<i>PCL_L_2_2</i>	-0.05	-2.67	150	0.008393	0.030816
<i>STG_R_6_5</i>	0.05	2.6	150	0.010194	0.036879
<i>LOcC_L_2_1</i>	0.05	2.6	150	0.010398	0.03707
<i>IFG_L_6_2</i>	0.05	2.58	150	0.010811	0.037992
<i>INS_L_6_3</i>	0.05	2.54	150	0.012239	0.042405
<i>BG_L_6_2</i>	0.08	2.51	150	0.01324	0.044767
<i>ITG_L_7_6</i>	0.05	2.5	150	0.013542	0.044767
<i>CG_L_7_2</i>	0.06	2.5	149	0.013585	0.044767
<i>BG_L_6_3</i>	0.09	2.5	150	0.013649	0.044767
<i>INS_L_6_6</i>	0.04	2.45	150	0.015355	0.049703
<i>Hipp_R_2_2</i>	0.08	2.45	150	0.015574	0.049757

*Note.* ROIs = Regions of Interest from the Brainnetome Atlas. The table shows the results of second-level group comparison (Group 3 > Group 1) for the average path distance (PL). *Beta* indicates the effect size (difference in PL between groups); *T* is the T-statistic from the general linear model; *dof* = degrees of freedom; *p-unc* = uncorrected *p*-value; *p*-values are two-tailed; *p-FDR* = *p*-value corrected for multiple comparisons using the false discovery rate (FDR).

## Appendix K Regions of Interest with a Significant Difference in Average Path Distance between Older Adults and Early Middle-Aged Adults

<i>ROI</i>	<i>beta</i>	<i>T</i>	<i>dof</i>	<i>p-unc</i>	<i>p-FDR</i>
<i>network</i>	0.03	1.75	145	0.081833	nan
<i>Amyg_L_2_1</i>	0.12	5.07	145	1e-06	0.000292
<i>Amyg_R_2_1</i>	0.11	4.55	145	1.1e-05	0.001406
<i>Tha_R_8_4</i>	0.12	4.42	145	1.9e-05	0.00156
<i>PhG_L_6_1</i>	0.16	4.03	144	9.1e-05	0.005204
<i>PhG_L_6_3</i>	0.09	3.93	145	0.000132	0.005204
<i>INS_L_6_1</i>	0.11	3.92	145	0.000137	0.005204
<i>INS_L_6_1</i>	0.08	3.88	145	0.000159	0.005204
<i>PhG_R_6_3</i>	0.11	3.86	145	0.000169	0.005204
<i>Tha_R_8_2</i>	0.11	3.57	145	0.000476	0.012781
<i>INS_L_6_5</i>	0.08	3.55	145	0.00052	0.012781
<i>MVOcC</i>	-0.09	-3.47	145	0.000695	0.01486
<i>L_5_3</i>					
<i>PhG_R_6_2</i>	0.14	3.46	142	0.000725	0.01486
<i>Hipp_L_2_1</i>	0.08	3.42	145	0.00081	0.015333
<i>PhG_R_6_6</i>	0.09	3.35	145	0.001045	0.018369
<i>INS_L_6_4</i>	0.09	3.31	145	0.001188	0.019482
<i>Tha_R_8_3</i>	0.14	3.27	143	0.00136	0.019777
<i>CG_R_7_2</i>	0.07	3.27	144	0.001367	0.019777
<i>OrG_L_6_2</i>	0.07	3.21	145	0.001655	0.022624
<i>Tha_L_8_5</i>	0.11	3.16	145	0.001937	0.024935
<i>INS_R_6_4</i>	0.07	3.14	145	0.002027	0.024935
<i>INS_R_6_5</i>	0.07	3.05	145	0.002721	0.031869
<i>INS_L_6_2</i>	0.1	3.03	144	0.002914	0.032589
<i>FuG_L_3_1</i>	0.07	2.99	145	0.003238	0.034631
<i>STG_R_6_5</i>	0.06	2.94	145	0.003859	0.039552
<i>STG_R_6_4</i>	0.05	2.89	145	0.004451	0.04073
<i>Hipp_R_2_2</i>	0.09	2.89	145	0.00448	0.04073
<i>ITG_L_7_1</i>	0.11	2.88	144	0.00459	0.04073
<i>FuG_R_3_1</i>	0.08	2.87	145	0.004765	0.04073
<i>INS_R_6_2</i>	0.15	2.86	145	0.004801	0.04073
<i>OrG_L_6_5</i>	0.11	2.84	144	0.005238	0.042953
<i>STG_R_6_3</i>	0.06	2.79	145	0.005937	0.047117
<i>STG_R_6_6</i>	0.04	2.76	145	0.006465	0.049697

*Note.* ROIs = Regions of Interest from the Brainnetome Atlas. The table shows the results of second-level group comparison (Group 3 > Group 2) for the average path distance (PL). *Beta* indicates the effect size (difference in PL between groups); *T* is the T-statistic from the general linear model; *dof* = degrees of freedom; *p-unc* = uncorrected *p*-value; *p*-values are two-tailed; *p-FDR* = *p*-value corrected for multiple comparisons using the false discovery rate (FDR).